Precipitation Characteristics in Eighteen Coupled Climate Models

AIGUO DAI

National Center for Atmospheric Research, Boulder, Colorado*

(Manuscript received 9 June 2005, in final form 21 December 2005)

ABSTRACT

Monthly and 3-hourly precipitation data from twentieth-century climate simulations by the newest generation of 18 coupled climate system models are analyzed and compared with available observations. The characteristics examined include the mean spatial patterns, intraseasonal-to-interannual and ENSO-related variability, convective versus stratiform precipitation ratio, precipitation frequency and intensity for different precipitation categories, and diurnal cycle. Although most models reproduce the observed broad patterns of precipitation amount and year-to-year variability, models without flux corrections still show an unrealistic double-ITCZ pattern over the tropical Pacific, whereas the flux-corrected models, especially the Meteorological Research Institute (MRI) Coupled Global Climate Model (CGCM; version 2.3.2a), produce realistic rainfall patterns at low latitudes. As in previous generations of coupled models, the rainfall double ITCZs are related to westward expansion of the cold tongue of sea surface temperature (SST) that is observed only over the equatorial eastern Pacific but extends to the central Pacific in the models. The partitioning of the total variance of precipitation among intraseasonal, seasonal, and longer time scales is generally reproduced by the models, except over the western Pacific where the models fail to capture the large intraseasonal variations. Most models produce too much convective (over 95% of total precipitation) and too little stratiform precipitation over most of the low latitudes, in contrast to 45%–65% in convective form in the Tropical Rainfall Measuring Mission (TRMM) satellite observations. The biases in the convective versus stratiform precipitation ratio are linked to the unrealistically strong coupling of tropical convection to local SST, which results in a positive correlation between the standard deviation of Niño-3.4 SST and the local convective-to-total precipitation ratio among the models. The models reproduce the percentage of the contribution (to total precipitation) and frequency for moderate precipitation (10–20 mm day^{-1}), but underestimate the contribution and frequency for heavy (>20 mm day^{-1}) and overestimate them for light (<10 mm day^{-1}) precipitation. The newest generation of coupled models still rains too frequently, mostly within the 1–10 mm day^{-1} category. Precipitation intensity over the storm tracks around the eastern coasts of Asia and North America is comparable to that in the ITCZ (10–12 mm day^{-1}) in the TRMM data, but it is much weaker in the models. The diurnal analysis suggests that warm-season convection still starts too early in these new models and occurs too frequently at reduced intensity in some of the models. The results show that considerable improvements in precipitation simulations are still desirable for the latest generation of the world's coupled climate models.

1. Introduction

Precipitation is one of the most important climate variables. The largest impact of future climate changes on the society will likely come from changes in precipitation patterns and variability. However, it is still a big challenge for coupled global climate models (CGCMs) to realistically simulate the regional patterns, temporal variations, and correct combination of frequency and intensity of precipitation (McAvaney et al. 2001; Covey et al. 2003; Trenberth et al. 2003; Meehl et al. 2005). The difficulty arises from the complexity of precipitation processes in the atmosphere that include cloud microphysics, cumulus convection, planetary boundary layer processes, large-scale circulations, and many others. Errors in simulated precipitation fields often indicate deficiencies in the representation of these physical processes in the model. It is therefore important to analyze precipitation for model evaluation and development.

* The National Center for Atmospheric Research is sponsored by the National Science Foundation.

Corresponding author address: A. Dai, National Center for Atmospheric Research, P.O. Box 3000, Boulder, CO 80307-3000.
E-mail: adai@ucar.edu

Previous analyses of model precipitation have mostly focused on mean patterns of precipitation amount (e.g., Hulme 1991; Srinivasan et al. 1995; Gates et al. 1999; Dai et al. 2001; Delworth et al. 2002; Covey et al. 2003; Rasch et al. 2006). However, precipitation is episodic and does not have continuous values like temperature and other climate variables. Precipitation can also have different types (e.g., convective versus stratiform) and phases (i.e., solid versus liquid). To fully characterize precipitation, it is necessary to examine its other properties, such as frequency and intensity, in addition to amount. Furthermore, detailed information regarding precipitation types (Dai 2001a), categories (e.g., light versus heavy; Sun et al. 2005), and diurnal variations (Dai 2001b) can also reveal deficiencies in various model physics such as moist convective and large-scale precipitation parameterizations.

It is known that most numeric weather and climate models tend to precipitate too frequently at reduced intensity, even though precipitation amount is reasonable (e.g., Chen et al. 1996; Osborn and Hulme 1998; Dai et al. 1999; Trenberth et al. 2003; Dai and Trenberth 2004; Sun et al. 2005). For example, Sun et al. (2005) show that over land most current CGCMs overestimate the frequency of light precipitation (1–10 mm day^{-1}) and underestimate the intensity of heavy precipitation (>10 mm day^{-1}). This problem is partly caused by the frequent firing of moist convection in models, whereas in nature the convective inhibition processes (e.g., large-scale subsidence) often allow atmospheric instability to accumulate before intense convection starts. Various approaches have been applied to alleviate this "drizzling" problem in models (e.g., Zhang 2003; Xie et al. 2004), but a full solution has proven to be difficult (Betts and Jakob 2002).

Another outstanding problem is the so-called double intertropical convergence zone (ITCZ; most evident over the tropical Pacific Ocean) phenomenon: there are two perennial zonal belts of maximum precipitation straddling the equator over the central and eastern Pacific Ocean in most CGCMs (Mechoso et al. 1995; Li et al. 2004), whereas in nature only during boreal spring is there a weak rainfall maximum south of the equator in the eastern Pacific (Lietzke et al. 2001; Zhang 2001; Gu et al. 2005). The rainfall double ITCZs in CGCMs are often accompanied by an equatorial cold tongue of sea surface temperature (SST) extending too far to the west in the Pacific (Mechoso et al. 1995). These equatorial rainfall and SST biases likely result from erroneous cloud feedbacks in the tropical Pacific (Sun et al. 2003; Dai et al. 2005), errors in equatorial west–east SST gradients and marine stratus clouds over the Peruvian coast (Li et al. 2004), and other air–sea interactions in CGCMs.

Here we analyze monthly, daily, and 3-hourly precipitation data from the twentieth-century climate simulations with 18 of the newest CGCMs, with data submitted to the Program for Climate Model Diagnosis and Intercomparison (PCMDI; see information online at http://www-pcmdi.llnl.gov/ipcc/about_ipcc.php) in support of the Intergovernmental Panel on Climate Change (IPCC) Fourth Assessment (AR4). We compare both among the models (and their previous versions) and with observations, focusing not only on mean spatial patterns, seasonal and year-to-year variations, but also on convective versus stratiform precipitation ratio, El Niño–Southern Oscillation (ENSO)-related variability, daily precipitation frequency and intensity for different precipitation categories, and the diurnal cycle. The results provide insight into the deficiencies (many of them are common among models) of the newest generation of CGCMs in the world. They are useful for model evaluation (e.g., for IPCC AR4) and development.

The paper is organized as follows: section 2 first describes the models, datasets, and analysis method. Section 3 discusses precipitation spatial patterns, whose associated biases in SST and cloud cover are described in section 4. Precipitation interannual variability is shown in section 5, while convective versus stratiform precipitation is discussed in section 6. Sections 7 and 8 discuss daily precipitation (frequency and intensity) and the subdaily (i.e., diurnal) variations, respectively. A summary is given in section 9.

2. Models, precipitation parameterizations, datasets, and analysis method

Table 1 summarizes the models whose twentieth-century climate simulations are used in this study. It includes all models [except a third version, Model-EH, from the Goddard Institute for Space Studies (GISS)] with data submitted to the PCMDI (as of March 2005), plus the Community Climate System Model, version 2 (CCSM2), whose precipitation diurnal cycle is included here. This newest generation of CGCMs has a generally increased resolution, and most of them [except for the Coupled Global Climate Model, version 3.1 (CGCM3.1), the Institute of Numerical Mathematics Climate Model (INM-CM; version 3.0), and the Meteorological Research Institute (MRI)-Coupled Global Climate model (CGCM; version 2.3.2)] do not use surface flux corrections. This is a big advance compared to the previous generation just a few years ago (e.g., Covey et al. 2003) where a majority of the models em-

TABLE 1. Climate models whose twentieth-century climate simulations were analyzed in this study.

Model name	Center/country	Atmospheric resolution (lat x lon)	Flux correction	Key reference
CCSM3	National Center for Atmospheric Research (NCAR)/United States	~1.4° × 1.4°	None	Collins et al. (2006)
CCSM2	NCAR/United States	~2.8° × 2.8°	None	Blackmon et al. (2001)
CGCM3.1	Canadian Centre for Climate Modelling and Analysis (CCCma)/Canada	~3.75° × 3.75°	Heat, water	Flato et al. (2000)
CNRM-CM3	CNRM/France	~2.8° × 2.8°	None	D. Salas-Mélia et al. (2006, personal communication)
CSIRO-Mk3.0	CSIRO/Australia	~1.88° × 1.88°	None	Gordon et al. (2002)
ECHAM5/MPI-OM	MPI/Germany	~1.88° × 1.88°	None	Roeckner et al. (2003)
FGOALS-g1.0	IAP/China	~2.8° × 2.8°	None	Yu et al. (2004)
GFDL-CM2.0	GFDL/United States	2.0° × 2.5°	None	Delworth et al. (2006)
GFDL-CM2.1	GFDL/United States	2.0° × 2.5°	None	Delworth et al. (2006)
GISS-AOM	GISS/United States	3.0° × 4.0°	None	Russell et al. (1995)
GISS-ER	GISS/United States	4.0° × 5.0°	None	Schmidt et al. (2006)
HadCM3	Met Office/United Kingdom	2.5° × 3.75°	None	Gordon et al. (2000)
HadGEM1	Met Office/United Kingdom	1.25° × 1.875°	None	Jones et al. (2005)
INM-CM3.0	INM/Russia	4.0° × 5.0°	Water [Greenland/Iceland/ Norwegian (GIN), Barentz and Kara Seas only]	Diansky and Volodin (2002)
IPSL-CM4	IPSL/France	~2.5° × 3.75°	None	Marti et al. (2005)
MIROC3.2- medres	Center for Climate System Research (CCSR)/National Institute for Environmental Studies (NIES)/Frontier Research Center for Global Change (FRCGC)/Japan	~2.8° × 2.8°	None	Hasumi et al. (2004)
MIROC3.2- hires	CCSR/NIES/FRCGC/Japan	~1.125° × 1.125°	None	Hasumi et al. (2004)
MRI-CGCM2.3.2a	MRI/Japan	~2.8° × 2.8°	Heat and water (global), momentum (12°S–12°N)	Yukimoto et al. (2006)
PCM	NCAR/United States	~2.8° × 2.8°	None	Washington et al. (2000)

ployed flux corrections in order to maintain a stable climate in their control runs. The highest atmospheric resolution is ~1.125° latitude × 1.125° longitude [the Model for Interdisciplinary Research on Climate (MIROC; version 3.2)-high resolution (hires)], which was unthinkable just 5–10 yr ago for CGCMs. The lowest resolution is 4.0° × 5.0° (GISS-ER and INM-CM3.0), while a majority of the models have a resolution of around 2°–3° or are approximately 200–300 km in grid size. Although the United States continues to have the largest number of CGCMs, Japan, France, China, and Russia have recently put more resources into climate modeling. Each of these countries now has one or more CGCMs. Some models listed in Table 1 are only slightly different versions, for example, MIROC3.2-medium resolution (medres) and MIROC3.2-hires differ only in resolution, while the Geophysical Fluid Dynamics Laboratory (GFDL)-Climate Model (CM; version 2.0) and GFDL-CM2.1 only have different numerical schemes for atmospheric advection. The GISS-Atmosphere–Ocean Model (AOM) and GISS-ER are, however, two very different models. All of the models include an ocean general circulation model (GCM) that often has higher horizontal resolution than the atmospheric GCM.

All of the models produce convective and stratiform (i.e., large scale) precipitation separately through cumulus convection and large-scale precipitation parameterizations (Table 2). Except for the lagged convective adjustment scheme (INM-CM3.0), the modified Emanuel (1991) scheme [Institut Pierre Simon Laplace (IPSL)-Climate Model (CM) 4], and the subgrid plume and buoyancy-based scheme (GISS-AOM), the deep convection schemes that produce convective precipita-

TABLE 2. Description of model parameterizations for stratiform (i.e., large scale) and convective precipitation.

Model name	Stratiform precipitation	Convective precipitation
CCSM3, CCSM2	Prognostic condensate and precipitation parameterization (Zhang et al. 2003)	Simplified Arakawa and Schubert (1974) (cumulus ensemble) scheme developed by Zhang and McFarlane (1995)
CGCM3.1	Precipitation occurs whenever the local relative humidity is supersaturated	Zhang and McFarlane (1995) scheme
CNRM-CM3	Statistical cloud scheme of Ricard and Royer (1993)	Mass flux convection scheme with Kuo-type closure
CSIRO-Mk3.0	Stratiform cloud condensate scheme from Rotstayn (2000)	Bulk mass flux convection scheme with stability-dependent closure (Gregory and Rowntree 1990)
ECHAM5/MPI-OM	Prognostic equations for the water phases, bulk cloud microphysics (Lohmann and Roeckner 1996)	Bulk mass flux scheme (Tiedtke 1989) with modifications for deep convection according to Nordeng (1994)
FGOALS-g1.0	Same as PCM	Zhang and McFarlane (1995) scheme
GFDL-CM2.0, GFDL-CM2.1	Cloud microphysics from Rotstayn (2000) and macrophysics from Tiedtke (1993)	Relaxed Arakawa–Schubert scheme from Moorthi and Suarez (1992)
GISS-AOM	Subgrid-relative humidity-based scheme	Subgrid plume and buoyancy-based scheme (online at http://aom.giss.nasa.gov/DOC4X3/ATMOC4X3.TXT)
GISS-ER	Prognostic stratiform cloud based on moisture convergence (Del Genio et al. 1996)	Bulk mass flux scheme by Del Genio and Yao (1993)
HadCM3	Large-scale precipitation is calculated based on cloud water and ice contents (similar to Smith 1990)	Bulk mass flux scheme (Gregory and Rowntree 1990), with the improvement by Gregory et al. (1997)
HadGEM1	Mixed phase cloud scheme (Wilson and Ballard 1999)	Revised bulk mass flux scheme
INM-CM3.0	Stratiform cloud fraction is calculated as linear function of relative humidity	Lagged convective adjustment after Betts (1986), but with changed referenced profile for deep convection
IPSL-CM4	Cloud cover and in-cloud water are deduced from the large-scale total water and moisture at saturation (Bony and Emmanuel 2001)	Moist convection is treated using a modified version (Grandpeix et al. 2004) of the Emanuel (1991) scheme
MIROC3.2-medres MIROC3.2-hires	Prognostic cloud water scheme based on Le Treut and Li (1991)	Prognostic closure of Arakawa–Schubert based on Pan and Randall (1998) with relative humidity–based suppression (Emori et al. 2001)
MRI-CGCM2.3.2a	Precipitation occurs whenever the local relative humidity is supersaturated	Prognostic Arakawa–Schubert based on Pan and Randall (1998)
PCM	Precipitation occurs whenever the local relative humidity is supersaturated	Zhang and McFarlane (1995) scheme

tion in most models are based the mass flux approach. This approach uses either spectral cloud ensemble models similar to Arakawa and Schubert (1974; hereafter AS) (e.g., GFDL-CM2.x, MIROC3.2, and MRI-CGCM2.3.2a) or a bulk cloud ensemble model [e.g., Centre National de Recherches Météorologiques (CNRM)-climate model, version 3 (CM3), Commonwealth Scientific and Industrial Research Organization (CSIRO)-Mark (Mk) 3.0, fifth-generation ECHAM (ECHAM5)/Max-Planck Institute (MPI)-Ocean Model (OM), GISS-ER, Hadley Centre Coupled Model, version 3 (HadCM3), and Hadley Centre Global Environmental Model (HadGEM1)]. In the bulk flux method, only one single cloud model is used to represent an average over all cloud types within a convective ensemble. Unlike the spectral method, the bulk method neither uses explicit assumptions on the mass and thermodynamic budgets of subensembles of cumulus clouds, nor provides information on the mass spectrum of various cloud types. Furthermore, the entrainment and detrainment rates in the bulk method are often set to correctly estimate the maximum cloud-top height, whereas they are dependent on the spectral cloud distribution in the spectral method. The two methods were shown to produce similar total vertical cloud mass fluxes for tropical convection (Yanai et al. 1976).

Several models [CCSM2, CCSM3, CGCM3.1, Flexible Global Ocean–Atmosphere–Land System (FGOALS)-grid point version (g1.0), and Parallel Climate Model (PCM)] use the Zhang and McFarlane (1995; hereafter ZM) scheme, which is somewhere between the spectral and bulk methods. It is based on the

same spectral rising plume concept as that in AS, and the bulk entrainment rate as a function of height is the same as that a spectral model would produce because the same spectral concept is used to estimate it. However, by assuming a constant spectral distribution in cloud-base mass flux, the thermodynamic equations were reduced to the bulk form in the ZM scheme. The ZM scheme is designed primarily for deep convection, whereas the conventional bulk flux schemes are designed to treat shallow, midlevel, and deep convection as a function of the cloud depth and the starting level.

Other important features of the cumulus parameterizations include closure assumptions, triggering mechanisms, and parameterization of convective-scale precipitation-driven downdrafts. Most schemes use a closure based on the assumption that convective available potential energy (CAPE) is consumed by cumulus convection over a given time scale (a few hours) (CAPE closure, e.g., ZM, ECHAM5). The AS schemes based on Pan and Randall (1998) employ a prognostic closure using the cumulus kinetic energy (e.g., MIROC3.2, MRI-CGCM2.3.2a). Some of the bulk mass flux schemes use a closure based on a stability-dependent mass flux (e.g., CSIRO-Mk3.0, GISS-ER). The primary triggering mechanisms in these cumulus schemes are based on either CAPE [or its equivalent cloud work function (CWF) in AS] or local parcel buoyancy. The former measures the instability based on the vertical integral of parcel buoyant energy, while the latter measures the instability by lifting a parcel through a specific distance or between two model layers. More information on these and other aspects of the cumulus parameterizations can be found in Xie et al. (2002) and the references given in Table 2.

Detailed information is difficult to obtain regarding how large-scale (i.e., stratiform) precipitation is produced in all of the models. In general, most models have prognostic treatment of cloud condensates from which grid-scale precipitation is derived (Table 2), while others (e.g., CGCM3.1, GISS-AOM, MRI-CGCM2.3.2a, and PCM) produce large-scale precipitation when relative humidity is supersaturated. Some models often execute the cumulus convection parameterization before the large-scale parameterization, but this information is unavailable for many of the models.

The twentieth-century climate simulations started from a condition of the late nineteenth century (mainly in terms of atmospheric contents of trace gases and solar irradiance) by branching out from a preindustrial control run. Historical time series (usually without spatial and seasonal variations) of atmospheric CO_2 and other greenhouse gases, sulfate aerosol direct effects, and volcanic and solar forcing were generally included in these model simulations, although specific treatments of these forcings vary among the models. The forcing differences should not affect our results because we focus on the climatologic patterns and variability.

We used monthly precipitation and other data from 1950 to 1999, daily precipitation data from 1950 to 1999 (available only for 12 models), and 3-hourly precipitation data from 1991 to 2000, which were available only for a small subset of the models (GISS-ER, GFDL-CM2.0/2.1, MIROC3.2-medres, MRI-CGCM2.3.2). For comparisons with observations, for example, from the Climate Prediction Center (CPC) Merged Analysis of Precipitation (CMAP; Xie and Arkin 1997) and the Global Precipitation Climatology Project (GPCP) Data Set-version 2 (Adler et al. 2003), we only used the time period with observations (i.e., 1979–99). In addition to the CMAP and GPCP monthly precipitation (on a 2.5° $\times$ 2.5° grid), we also used GPCP pentad (i.e., 5-day averaged) precipitation from 1970 to 1999 (also on a 2.5° $\times$ 2.5° grid) for evaluating variability on intraseasonal and shorter time scales.

In extratropical cyclones and tropical regions with old and weak convection (alongside young, vigorous convective cells), precipitation produces layered radar echoes and is usually called "stratiform"; whereas precipitation generated by vigorous convection produces vertically oriented cells of high reflectivity and is called "convective" (Houze 1997). Global observations of the two types of precipitation are sparse. Dai (2001a) shows global seasonal maps of showery (a proxy of convective) and nonshowery (a proxy of stratiform) precipitation frequency based on surface weather reports. Recent spaceborne precipitation radar measurements from the Tropical Rainfall Measuring Mission (TRMM) (Kummerow et al. 2000) have been used to separate the convective component (produced within small regions around convective centers in the Tropics) from the rest of the precipitation (produced within a large background region) using an algorithm based on the vertical profile of reflectivity and the horizontal variability of the echo (Awaka et al. 1997; Schumacher and Houze 2003). Although the TRMM separation scheme is qualitatively consistent with the fact that models produce convective precipitation from subgrid-scale moist convection and the rest of the precipitation comes from grid-scale processes, the definition of these two types of precipitation is not fully comparable between the models and observations from TRMM and weather reports, or even among the models. Furthermore, it has been shown (Biggerstaff and Listemaa 2000) that the TRMM rain-type algorithm for ground-

based validation sites may incorrectly classify the rain types for 14% of the rain amount, although this error varies with individual storm systems. Nevertheless, it is worthwhile to examine convective and stratiform components of the total precipitation because these two types of precipitation have very different mass and heating profiles, which have important implications for atmospheric circulation and thermodynamics (Houze 1997; Schumacher et al. 2004). Therefore, we used the TRMM convective and stratiform precipitation rate data (product 3A25, 37°S–37°N, 0.5° grid, 1998–2004) together with the showery and nonshowery precipitation frequency data from weather reports (Dai 2001a) for higher latitudes as an approximate measure of fractional contributions by the two types of precipitation.

The 3-hourly merged precipitation product from TRMM (3B42 version 6, 50°S–50°N, 0.25° grid, 1998–2003; see online at http://lake.nascom.nasa.gov/data/dataset/TRMM/01_Data_Products/02_Gridded/index.html), together with the 3-hourly surface weather reports (Dai 2001b), were used to evaluate the diurnal cycle in the model-simulated precipitation. The TRMM 3-hourly precipitation data were derived by using an optimal combination of TRMM and other microwave [the Special Sensor Microwave Imager (SSM/I), Advanced Microwave Scanning Radiometer (AMSR), and Advanced Microwave Sounding Unit (AMSU)] precipitation estimates to adjust infrared radiation (IR) estimates from geosynchronous satellite IR observations. We simply averaged the all TRMM datasets to a 2.5° × 2.5° grid for calculations that are sensitive to spatial resolution (e.g., precipitation frequency and intensity). This increases the comparability with the model precipitation. We did not attempt to remap the model fields to have the same grid size because our focus is on large-scale variations, and the difference in the model resolution has only small effects on the results.

The 3-hourly data were first stratified by season and then averaged over the days and years for each 3-h period to derive composite seasonal-mean diurnal cycles. Then, the amplitude and phase of the diurnal (24 h) harmonic were estimated based on the composite diurnal curves at each grid box. More details of the diurnal analysis can be found in Dai et al. (1999) and Dai (2001b).

To save space and be concise, we only show results for selected models in some of the figures. In these plots, the models are selected either to show the worst, best, and average cases or are popular in the literature. In most of the cases, we mention the other models in the text or in figure captions.

3. Precipitation spatial patterns

Figure 1 compares the mean spatial patterns of annual precipitation from observations (CMAP[1]) and 13 models. Here we focus on the Tropics and subtropics, such as the rainbelts in the Pacific (for high-latitude land areas, see Sun et al. 2005). Most models reproduce the observed broad patterns, such as the heavy rainfall around the Indonesia region, a narrow belt of maximum rainfall (i.e., the ITCZ) north of the equator, and the dry areas over the subtropical pressure highs and in northern Africa and the Middle East. Considerable differences exist, however, between the observations and the models and among the models themselves. For example, the double-ITCZ pattern is still evident in most of the models (in both annual and seasonal precipitation) except for two flux-corrected models (CGCM3.1 and MRI-CGCM2.3.2) and GISS-ER, which has an unrealistic broad rainbelt across the entire tropical Pacific. The double ITCZs are particularly pronounced in INM-CM3.0 and CNRM-CM3. Several models (e.g., CSIRO-Mk3.0, GFDL-CM2.1, INM-CM3.0) are too dry over tropical America, including the Amazon. Substantial biases are also evident over the tropical Atlantic Ocean, for example, the subtropical dry areas extend too far west and equatorward in many models. Tropical precipitation patterns from many new models, such as the HadGEM1 and CCSM3, have no substantial improvements over their previous generations, such as the HadCM3 and Climate System Model (CSM), version 1 (Dai et al. 2001), respectively. The MRI-CGCM2.3.2 has the most realistic precipitation pattern at low latitudes among the models, probably owing to its use of monthly climatologic flux corrections. Among the models without flux correction, MIROC3.2 (both the T42 and T106 versions) and HadCM3 produce relatively good precipitation patterns. The fact that models with surface flux corrections produce fairly realistic rainfall patterns suggests that errors in air–sea interactions (i.e., heat, water, and momentum exchanges) and associated positive feedbacks amplify SST and rainfall biases in the Tropics and contribute to the double-ITCZ problem. More detailed analyses of the causes of the rainfall double ITCZs are out of the scope of this study.

[1] Note that the GPCP v2 has spatial patterns similar to CMAP. The main differences include that the CMAP has higher oceanic precipitation (cf. Fig. 2) due to its calibration with rainfall data from over 100 coastal and atoll rain gauges (Xie and Arkin 1997), while the GPCP v2 has higher precipitation over land during cold months due to its climatologic correction for wind-induced undercatch by rain gauges (Adler et al. 2003).

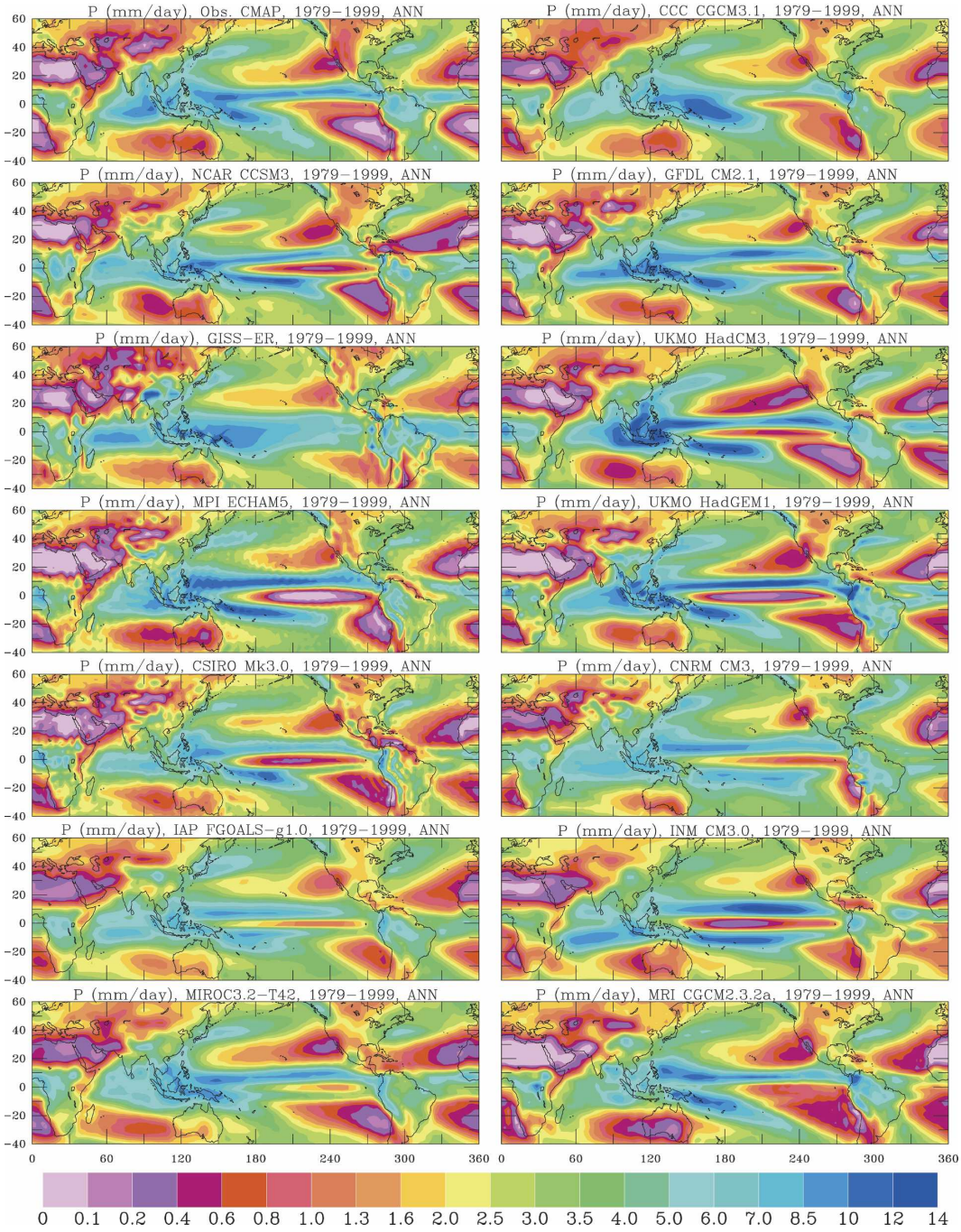

FIG. 1. 1979–99 mean annual precipitation from observations (CMAP; Xie and Arkin 1997) and twentieth-century climate simulations by 13 coupled climate models.

Latitudinal distributions of zonal-mean precipitation and their seasonal variations are broadly captured by most of the models (Fig. 2). In particular, the peak ITCZ rainfall and its seasonal migration (from ~7.50°S in January to 8.25°N in July, with an annual mean of ~6.75°N) are reproduced by most of the models. Figure 2 shows that current observational precipitation products have large uncertainties, mainly because of wind-induced undercatch by rain gauges and uncertainties in oceanic precipitation estimates. These observational uncertainties are comparable to the spread among the models at most latitudes, except for the peak south of the equator, where most models substantially overestimate the rainfall in both January and July and in annual

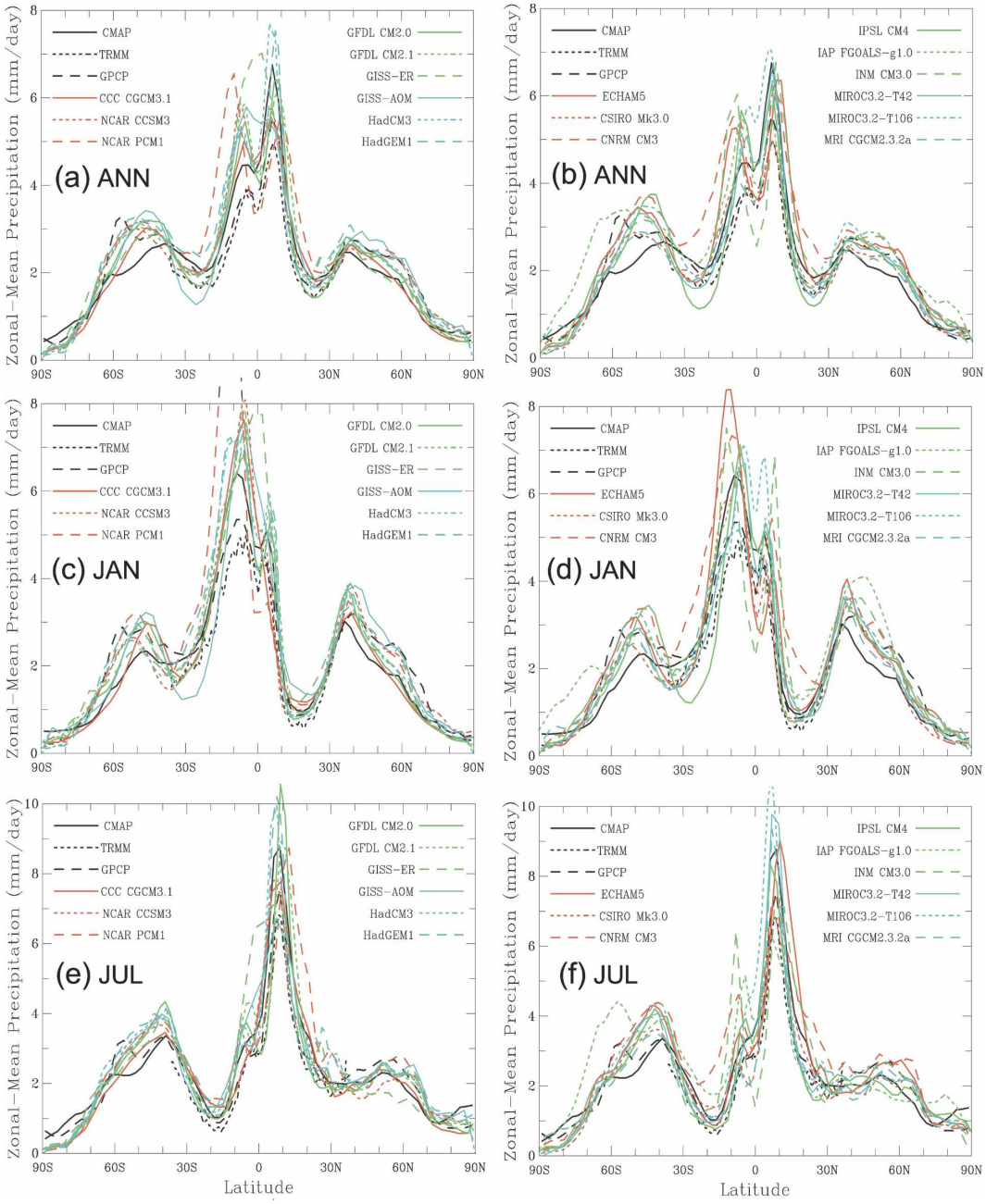

FIG. 2. Latitudinal distribution of zonally averaged precipitation for (a),(b) annual, (c),(d) January, and (e),(f) July mean from three observational analyses (CMAP, GPCP, and TRMM, black lines) and twentieth-century climate simulations by 18 CGCMs (colored lines). All data were averaged over the 1979–99 period except for TRMM, which is the 1998–2003 mean.

mean, compared with all three data products (CMAP, GPCP v2, and TRMM) (Fig. 2). Model precipitation is closer to GPCP v2 than CMAP at mid- and high latitudes, as the GPCP v2 has been corrected for wind-induced undercatch by rain gauges. At low latitudes, however, most models are closer to the CMAP, which has higher tropical precipitation (owing to its calibration to coastal and atoll rain gauges) than GPCP v2 and TRMM.

To reveal longitudinal variations in the annual cycle, Fig. 3 shows the latitude–month plots of monthly precipitation averaged over six different longitude sectors from CMAP and one of the better and worse models, and the average of the 18 models. The north–southward

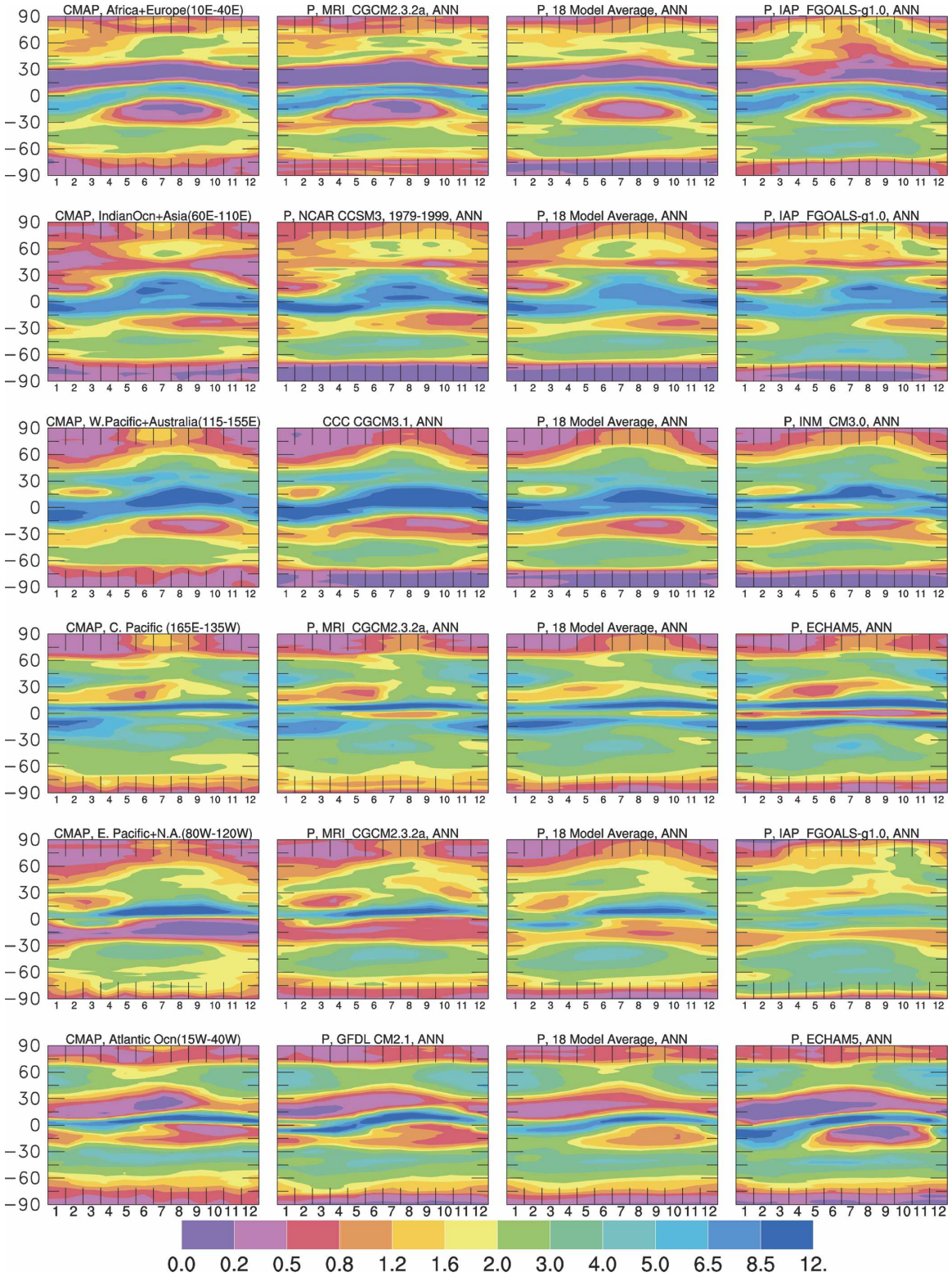

FIG. 3. Zonally averaged precipitation (mm day^{-1}) as a function of latitude (vertical coordinate, negative for the Southern Hemisphere) and month averaged over 1979–99 from (left) observations (CMAP) and (second column from left) one of the better and (right column) worse model simulations, together with the (third column) average of the 18 models. The zonal averaging was done for six longitude sectors (from top to bottom): Africa and Europe (10°–40°E), the Indian Ocean and Asia (60°–110°E), the western Pacific Ocean and Australia (115°–155°E), the central Pacific (165°E–135°W), the eastern Pacific and North America (80°–120°W), and the Atlantic Ocean (15°–40°W).

seasonal migration of the rainbelt varies greatly among the sectors. For example, over the central Pacific, the ITCZ is located around 5°–8°N all year around, whereas it migrates from 2°–15°S in January to 10°–18°N in August in the western Pacific/Australia sector (115°–155°E). The ITCZ also migrates considerably in the Atlantic and Indian Ocean sectors. The models generally reproduce these seasonal movements, but large errors are evident over the central Pacific Ocean where a heavy rainbelt exists south of the equator all year around in contrast to just winter and spring in observations. Some models (e.g., FGOALS-g1.0) also fail to simulate the seasonal cycle over Eurasia.

4. SST and cloudiness biases

The above model deficiencies in tropical precipitation are related to biases in SST fields (Fig. 5), as in previous generations of CGCMs (e.g., Mechoso et al. 1995). The flux-corrected models (CGCM3.1 and MRI-CGCM2.3.2a) have the most realistic SST patterns in the Tropics, although Atlantic SST in CGCM3.1 is too warm off equatorial Africa. The cold tongue of SST in the equatorial eastern Pacific extends to the central Pacific in most models, such as CCSM3, GFDL-CM2.1, ECHAM5, HadGEM1, CSIRO-Mk3.0, CNRM-CM3, INM-CM3.0, and MIROC3.2, while GISS-ER does not have a SST cold tongue at all [SST over the cold tongue region in GISS-AOM is also too warm (over 27°C)]. Associated with this extended SST cold tongue, an unrealistic narrow band of minimum precipitation exists over the equatorial central and eastern Pacific in all these models (Fig. 1). This minimum rainbelt is an integral part of the double-ITCZ pattern. On the other hand, the SST cold tongue does not extend to the coast of South America as in observations in many models, such as FGOALS-g.10 and HadCM3, and, to a lesser extent, GFDL-CM2.1 and CCSM3. The SST biases along coastal South America are likely related to weak oceanic upwelling and biases in marine stratus clouds, while the SST errors in the central Pacific may be related to errors in cloud radiative feedbacks, as shown in an earlier version of the atmospheric model of the CCSM3 by Sun et al. (2003).

In addition to the cold tongue errors, some models, such as HadCM3, FGOALS-g1.0, and ECHAM5, have a warm SST bias, especially over the western Pacific and Indian Oceans, while others (e.g., CNRM-CM3, MIROC3.2, CSIRO-Mk3.0, and HadGEM1) have cold biases. The warm SST in the HadCM3 is associated with excess tropical precipitation, and the cold SST in the CNRM-CM3, MIROC3.2, and CSIRO-Mk3.0 is associated with negative precipitation biases in these models (Fig. 1). However, the FGOALS-g1.0 has a warm SST bias, but its tropical precipitation is actually below that observed (Fig. 1). Thus, tropical precipitation amount is not always determined by tropical SST among different models, although within individual models the SST and precipitation patterns are positively correlated in the Tropics.

Large SST biases are also seen over the tropical Atlantic Ocean in many models (Fig. 4). For example, SST in CNRM-CM3 HadGEM1, and INM-CM3.0 is 1°–2°C colder than that observed and has incorrect spatial patterns and gradients, a deficiency found in many previous CGCMs (Davey et al. 2002). Furthermore, SST in the Caribbean Sea and Gulf of Mexico has cold biases in most models except for MRI-CGCM2.3.2a, HadCM3, and ECHAM5. The SST biases are consistent with the dry biases in the Caribbean Sea and surrounding regions in many of the models (cf. Fig. 1).

As stated above, the tropical SST and thus precipitation biases may be related to errors in simulated clouds. Most models indeed have large biases in the distribution of mean total cloud amount (plot not shown), as shown in earlier studies (e.g., Dai and Trenberth 2004; Li et al. 2004). In particular, the widely used HadCM3 and its newer version HadGEM1 severely underestimate cloud cover over most of the globe, especially over low-latitude oceans, as shown by Martin et al. (2004). The MIROC3.2, which has a relatively realistic precipitation field among the CGCMs without flux corrections (Fig. 1), also underestimates cloud amount, especially over the subtropical oceans. On the other hand, the CSIRO-Mk3.0 and FGOALS-1.0g considerably overestimate the cloud amount in the Tropics. Another common bias is that subtropical marine stratus clouds off the western coasts of the Americas and Africa are often underestimated in most models, except INM-CM3.0. The CGCM3.1 and GISS-ER have relatively realistic cloud distributions. Although total cloud cover is just one of many cloud properties that can influence clouds' effects on surface radiative fluxes and thus temperature, it is necessary for models to produce the right cloud amount in order for them to simulate the surface fluxes correctly for the right reason.

5. Precipitation variability

Figure 5 shows the standard deviation (sd) of annual precipitation calculated using a 24-yr period from CMAP and GPCP v2 (1979–2002) and six selected models (1976–99). The models generally reproduce the broad patterns of sd, with better sd fields found in models with more realistic mean precipitation distributions.

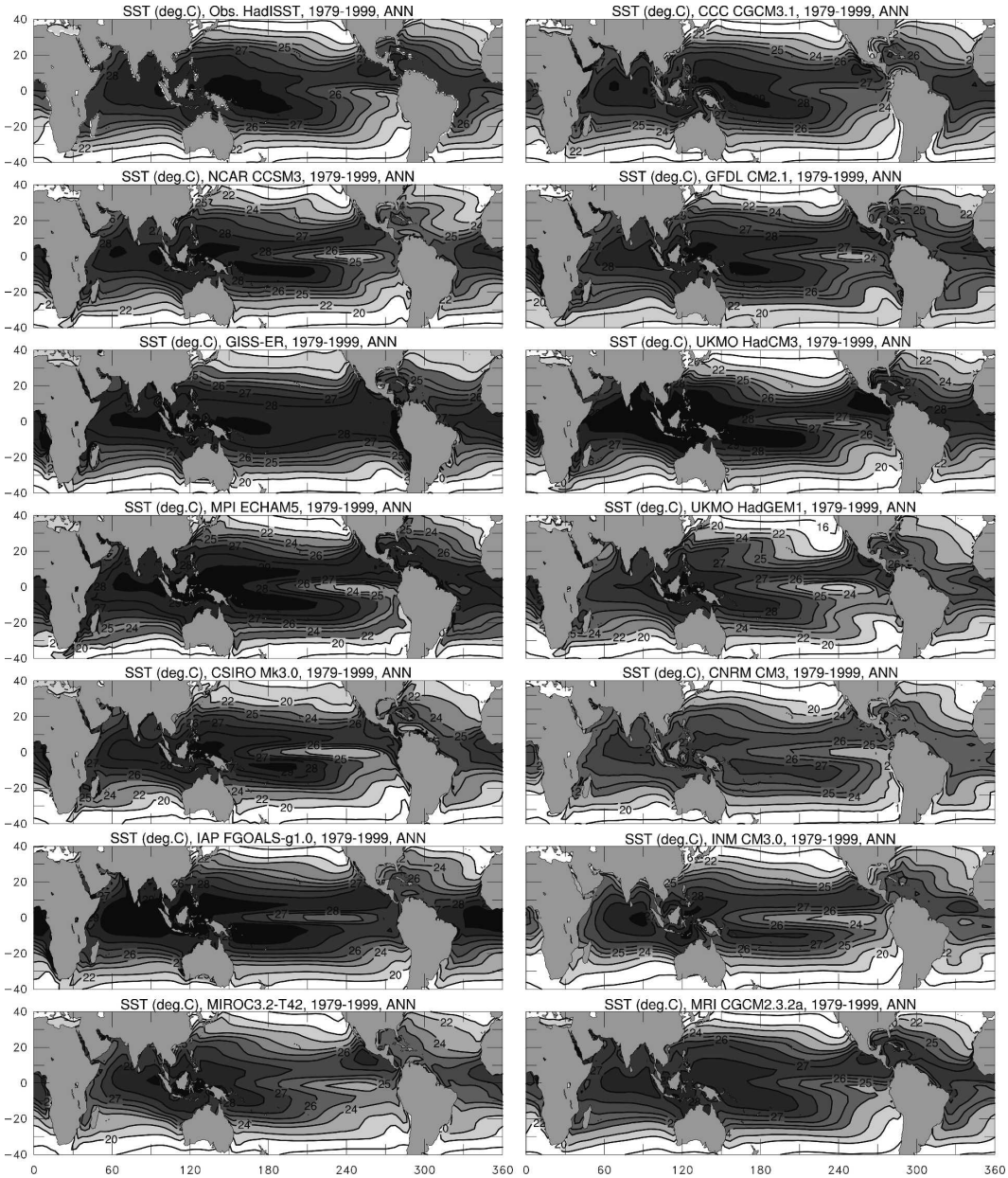

FIG. 4. 1979–99 mean annual SST from observations (HadISST; Rayner et al. 2003) and twentieth-century climate simulations by 13 coupled climate models. Contour levels are 16°, 20°, 22°, 24°, 25°, 26°, 27°, 28°, 29°, and 30°C.

The GFDL-CM2.1 and -CM2.0 both overestimate the sd in the equatorial central and western Pacific, while the GISS models (especially GISS-AOM, cf. Fig. 6) considerably underestimate tropical precipitation variability. This problem in GISS-ER is unlikely owing only to its relatively low resolution (4° × 5°), as the GISS-AOM (with a higher resolution) has an even lower sd and the INM-CM3.0 (also 4° × 5°) has more realistic tropical precipitation variability (not shown).

Percentage contributions of bandpassed variations to the total variance (calculated using pentad precipitation data) are shown in Figs. 6–7. The intraseasonal (20–80 day) variations account for the largest (20%–40%) percentage, while the interannual variations contribute very little (<5%), except over the tropical Pacific where they are significant (10%–15%), resulting from ENSO. Seasonal (80–365 day) variations contribute 5%–20% to the total variance. The models reproduce the general partitioning, with substantial biases in South America and the tropical Pacific.

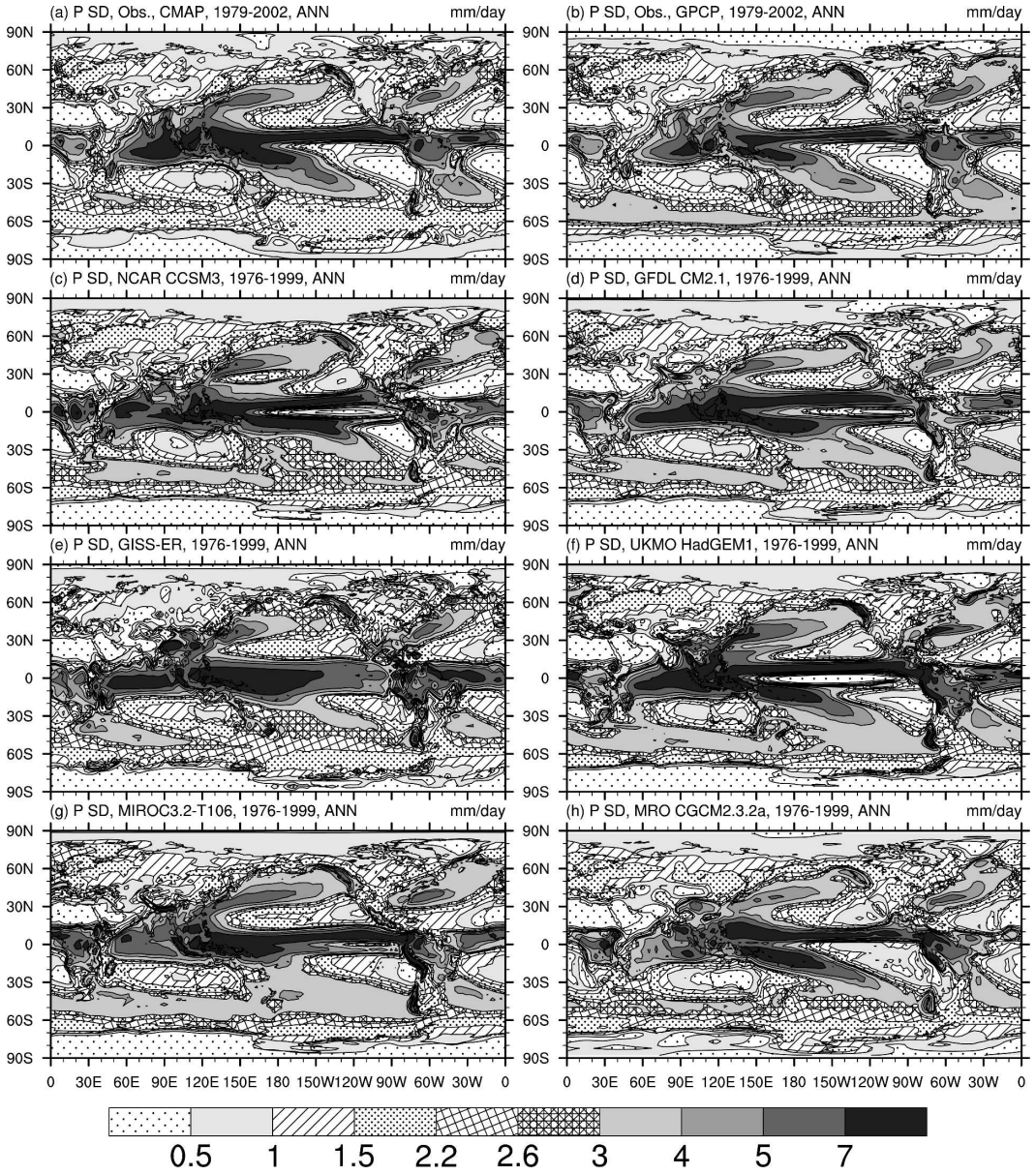

FIG. 5. Standard deviation of annual precipitation (mm day^{-1}) from CMAP and GPCP v2 (1979–2002) and six selected CGCMs (1976–99).

Figure 8 shows the power spectra of GPCP pentad and model-simulated daily precipitation for six oceanic and six land regions. Except for the western Pacific, where ENSO induces peak power of around 2–7-yr time scales, the largest peak of power is for the annual cycle. A secondary peak is evident at the semiannual time scale for some low-latitude regions (e.g., the subtropical South Pacific and Amazon). The models reproduce the general features of the observed spectra, although the semiannual cycle of precipitation over the tropical eastern Pacific, Amazon, and India is slightly stronger than observed. Over the western Pacific, the GPCP precipitation shows substantial power at the intraseasonal (20–80 day) time scales, which the models fail to capture (Figs. 8A1 and 8B1).

ENSO has the single largest influence on precipitation at low latitudes on interannual-to-multiyear time scales in observations (e.g., Dai et al. 1997; Dai and Wigley 2000). An empirical orthogonal function (EOF) analysis of SST and precipitation revealed (not shown) that one of the leading EOFs of low-latitude rainfall (5%–10% variance) is related to tropical Pacific SST

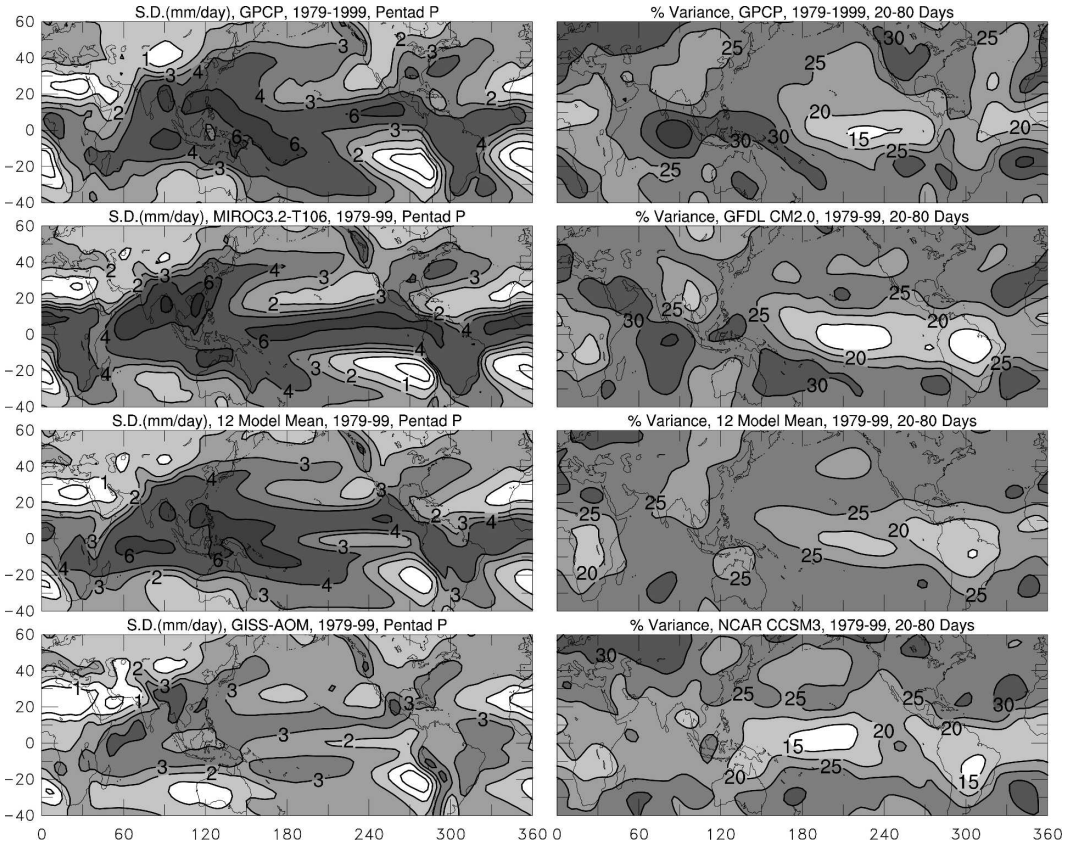

FIG. 6. (left) Standard deviation (mm day^{-1}) of pentad (i.e., 5-day average) precipitation during 1979–99 from (top) an observational analysis (GPCP), (second row) one of the better model simulations, (third row) 12 model mean, and (bottom) one of the worse model simulations. (right) Same as the left column, except for percentages of the total variance of the pentad precipitation (i.e., squared sd shown in the first column) explained by the variations on intraseasonal time scales (20–80 days). Note the better (second row) and worse (bottom row) cases may vary in different columns.

variations in most of the models, although the representation of the ENSO SST variability varies among the models (also see Monahan and Dai 2004). Here we simply use the mean SST averaged over the Niño-3 and -4 regions (5°S–5°N, 160°E–90°W) to represent ENSO variations and correlate this SST time series with local precipitation to illustrate the ENSO-related precipitation patterns (Fig. 9). As shown by Doherty and Hulme (2002), many models, especially the GFDL-CM2.1, HadCM3, and ECHAM5, reproduce the horseshoe-shaped pattern originating from the Indonesia region and extending northeast- and southeastward. Some models show too strong a correlation over tropical Central and South Americas (e.g., GFDL-CM2.1, HadCM3, and ECHAM5) and the southern Indian Ocean (MIROC3.2), while the correlation over the tropical eastern Pacific is generally too weak. ENSO-related precipitation variability is too small in the GISS-ER with little correlation over Australia and the Indonesia region.

6. Convective versus stratiform precipitation

Figures 10–11 compare the model-simulated stratiform precipitation and convective-to-total (PRC/PR) precipitation ratio with those from TRMM (for 37°S–37°N) and surface observations (outside 37°S–37°N). The MIROC3.2, CGCM3.1, and, to a lesser degree, GISS-ER produce relatively realistic stratiform precipitation fields, whereas all of the other models produce too little stratiform and too much convective precipitation compared with these observational estimates. This is especially true for the GFDL and Met Office models, GISS-AOM, and PCM (not shown), in which over 95% of the total precipitation comes from convection over most of the low latitudes, compared with 45%–65% in the TRMM data (excluding the subtropical dry areas) (Fig. 11). Although the TRMM and surface observations likely contain uncertainties, the very high convective-to-total precipitation ratio (>90%) suggests that

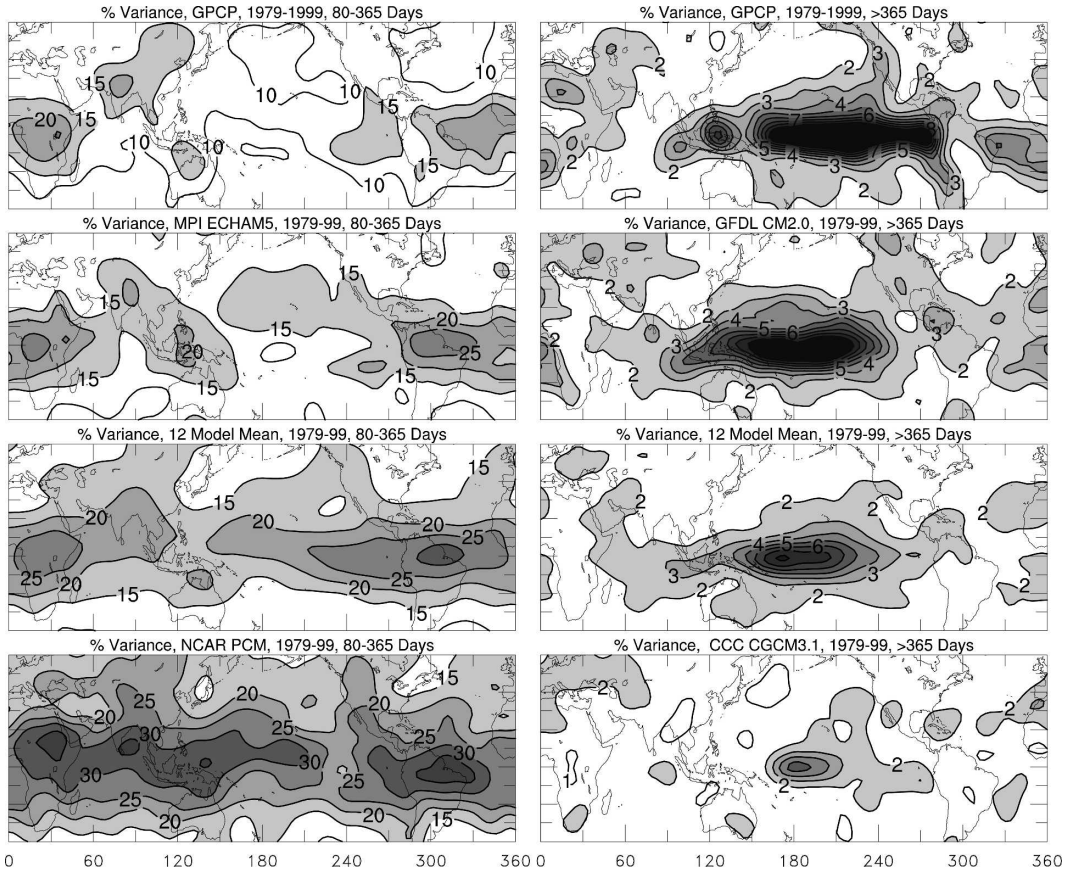

FIG. 7. Same as the right column of Fig. 6, except for (left) seasonal (80–365 days) and (right) interannual (>365 days) variations.

most current CGCMs derive their tropical precipitation through an incorrect combination of precipitation types.

The biases in the convective versus stratiform precipitation ratio may have significant impacts on other aspects of the simulated climate because of their different heating profiles and other characteristics (Houze 1997; Schumacher et al. 2004). For example, Fig. 12 shows that the sd of the annual SST averaged over the Niño-3.4 region (5°S–5°N, 120°–170°W, with similar results for Niño-3 and -4 regions) increases with the mean PRC/PR ratio averaged over the same region among the models when a few outlier models (GISS-ER, GISS-AOM, and FGOALS-g1.0) are excluded. As usual, the models scatter around the observations, with the MIROC3.2 at the low end and the GFDL-CM2.1 and CNRM-CM3 at the high end. This intermodel relationship between the ENSO SST amplitude and the PRC/PR ratio is also seen within the CGCM3.1 model when parameterizations were changed to alter the PRC/PR ratio (W. J. Merryfield 2005, personal communication). Thus, there is evidence that ENSO amplitudes increases with the PRC/PR ratio among different models and within individual models.

The positive correlation between Niño-3.4 SST and the PRC/PR ratio is also evident among their seasonal anomalies in most of the models (Fig. 13). This suggests that in the models tropical convection is strongly coupled to local SST so that warmer SST produces more vigorous convection and thus more convective (and less stratiform) precipitation. However, the limited TRMM PRC/PR data (from 1998 to 2004) and the Hadley Centre Sea Ice and Sea Surface Temperature (HadISST) data show a negative correlation for seasonal anomalies (Fig. 13a). These results suggest that in most models tropical oceanic convection is too strongly coupled to local SST, and this unrealistic coupling produces the intermodel relationship between ENSO SST amplitude and the PRC/PR ratio (shown in Fig. 12).

7. Daily precipitation frequency and intensity

Figure 14 shows the long-term mean distribution of annual frequency and intensity of daily precipitation

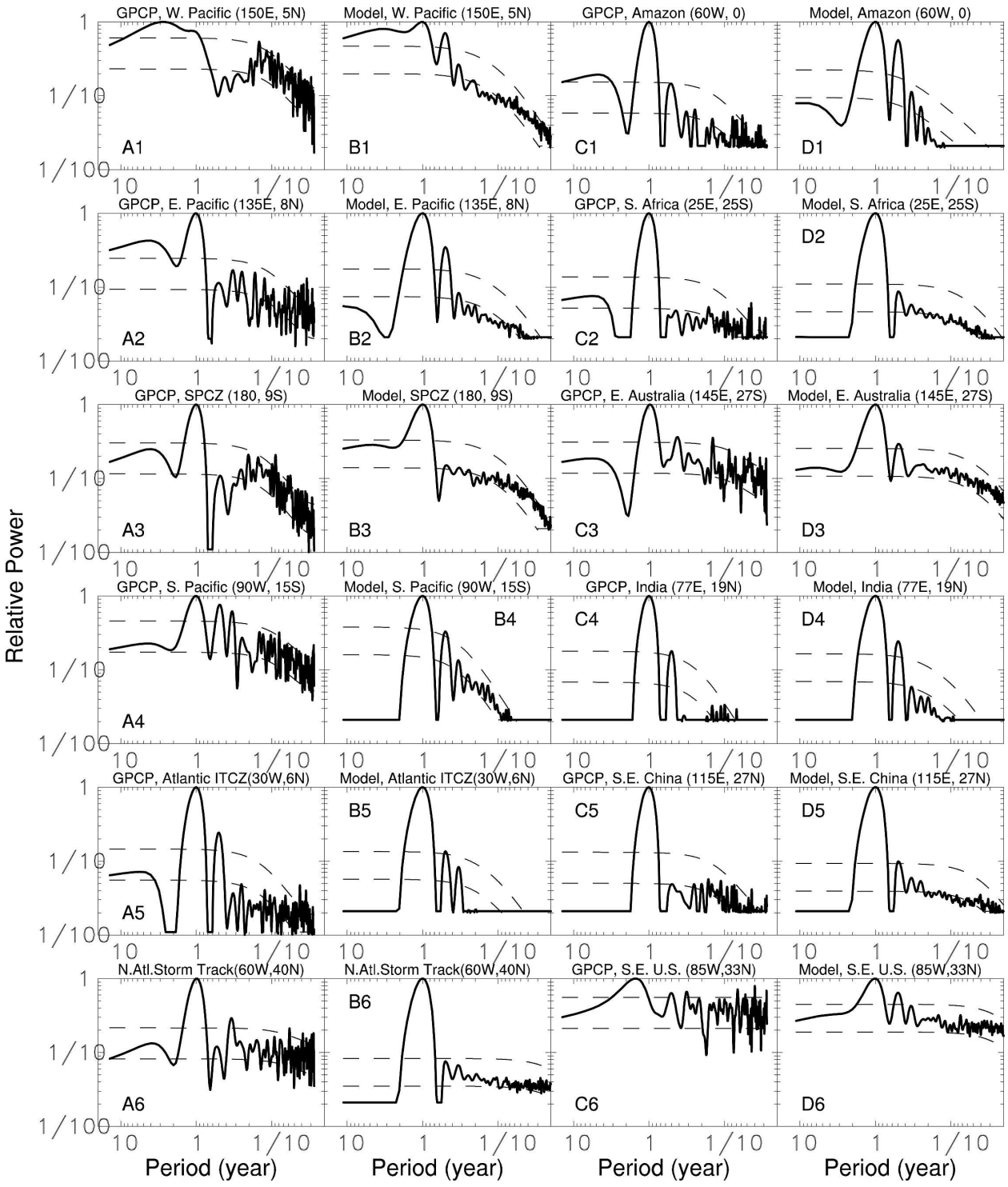

FIG. 8. Normalized power spectra of observed pentad (from GPCP; columns A and C) and model-simulated daily (columns B and D) precipitation from six oceanic regions (10° lat × 10° lon with the center shown at the top; columns A and B) and six land regions (6° lat × 6° lon; columns C and D) during 1979–99. The mean of the power spectra from 12 models is normalized by the largest peak and then is shown here in logarithmic scales. The thin dashed lines are 5% and 95% confidence limits.

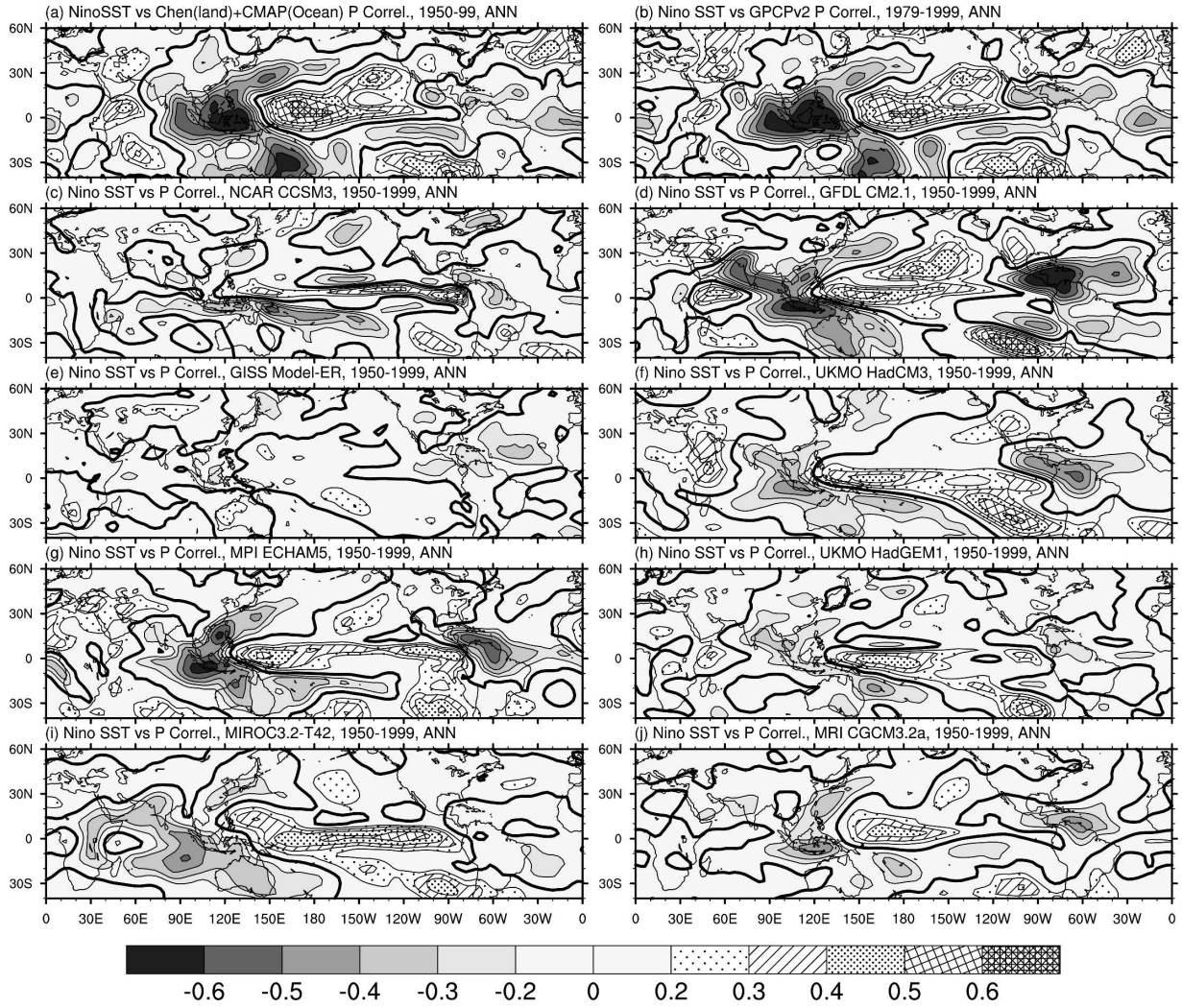

FIG. 9. Maps of correlation coefficients between annual ENSO index (SST averaged over 5°S–5°N, 160°E–90°W) and annual precipitation at each grid box in observations (top) of SST from HadISST and precipitation from (top left) CMAP (for oceans from 1979–99) and Chen et al. (2002) (for land from 1950–99) and (top right) GPCP v2 from 1979–99 and eight coupled models (both SST and precipitation are from IPCC AR4 twentieth-century simulations from 1950–99).

calculated using the 3-hourly data from TRMM and four models (GFDL-CM2.0, GISS-ER, MIROC3.2, and MRI-CGCM2.3.2a). Here precipitating days are defined as days with daily total precipitation exceeding 1 mm day^{-1}, the frequency is the number of precipitating days as a percentage of the number of all days with data, and the intensity is the mean precipitation rate averaged over all precipitating days. The frequency and intensity were computed at each box for each year and then averaged over all of the years.

The TRMM data (Fig. 14) show that daily precipitation intensity is relatively uniform (~3–6 mm day^{-1}) over most land areas, whereas over the oceans it is around 10–12 mm day^{-1} in the rainbelts (cf. Fig. 1) and 5–8 mm day^{-1} over the rest of the oceans, except for the subtropical highs where it is around 1.5–3.0 mm day^{-1}. On the other hand, daily precipitation frequency is more variable spatially, ranging from less than 5% in the Sahara, the Middle East, Mongolia, and the subtropical highs over the oceans, to ~65% in the ITCZ and 70%–80% in northern South America and Indonesia. Daily precipitation over the storm tracks around the eastern coasts of Asia and North America has intensity comparable to that in the ITCZ, but with a much lower frequency (~35%–50%) (Fig. 14), which results in a substantially lower precipitation amount in these regions than in the ITCZ (cf. Fig. 1).

The GISS-ER severely overestimates the precipitation frequency and underestimates the intensity over the oceans, while the other three models reproduce the

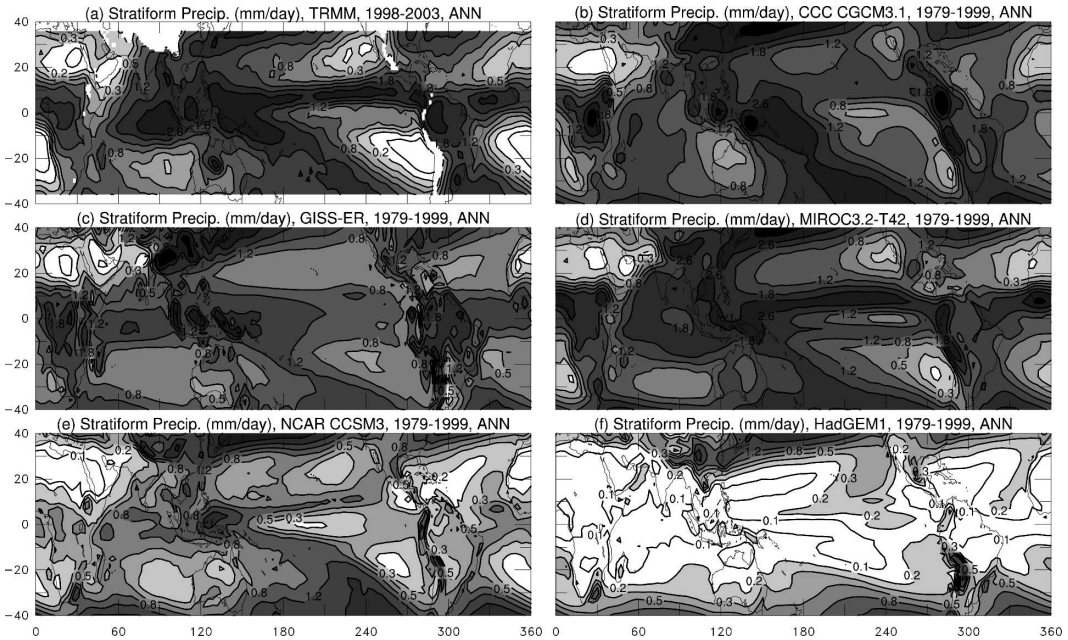

FIG. 10. Annual stratiform precipitation (mm day^{-1}) from TRMM 3A25 dataset (1998–2003 mean, 37°S–37°N) and five CGCMs (1979–99 mean). The GFDL-CM2.0, GFDL-CM2.1, GISS-AOM, HadCM3, and PCM are similar to HadGEM1, while the other models of Table 1 (not shown here) are somewhere between the CCSM3 and HadGEM1.

broad patterns (Fig. 14). However, these models also slightly underestimate the intensity and overestimate the frequency over the oceans. The tropical high-intensity bands are too narrow and confined in the models. The high-intensity bands associated with the storm tracks around the eastern coasts of Asia and North America are too weak and their patterns are not well simulated by the models.

To examine the frequency and intensity deficiencies in more detail, we calculated the frequency and intensity for different precipitation categories (from >0 to 1, 1–5, 5–10, 10–20, 20–50, and >50 mm day^{-1}). Figure 15 shows the histograms[2] of area-averaged (for 50°S-50°N, similar for other zones) annual frequency and percentage contribution to the total precipitation amount by individual precipitation categories. Note that Fig. 15b (frequency) is on a logarithmic scale, and that columns within each category are for, from left to right, TRMM, GFDL-CM2.0, GISS-ER, MIROC3.2-T42, and MRI-CGCM2.3.2a.

For the percentage contribution, the models derive their precipitation heavily from the 1–5 mm day^{-1} category (28%–38%, cf. 19% in TRMM data), while the TRMM data show the largest contribution (25%, cf. 6%–16% for the models) from precipitation within 20–50 mm day^{-1} (Fig. 15a). The TRMM observations derive 7% of the total precipitation from very heavy rainfall (>50 mm day^{-1}), in contrast to 0%–2% for the models. On the other hand, the models derive 12%–14% of their precipitation from drizzles (≤1 mm day^{-1}), compared with 8% in the TRMM data. For moderate precipitation (10–20 mm day^{-1}), the model-simulated percentage contributions are comparable to the TRMM data.

The above partitioning biases are also reflected in the histogram of precipitation frequency (Fig. 15b). For heavy precipitation (>20 mm day^{-1}), the models underestimate the frequency substantially (note the logarithmic scale). For example, for very heavy precipitation (>50 mm day^{-1}), the TRMM data show a frequency of 0.35%, whereas it is 0.02%–0.11% for the models. For the 20–50 mm day^{-1} category, the frequency is 2.78% for TRMM and 0.97%–2.13% for the models. Surprisingly, the frequency for the very light precipitation (from nonzero to 1 mm day^{-1}) is reasonable (45.9% for TRMM and 37.4%–59.8% for the models), but the models overestimate the frequency for precipitation within 1–10 mm day^{-1}, which is consistent with an analysis of model-simulated land precipitation by Sun et al. (2005). The models tend to have nonzero precipitation nearly every day (84%–100% of the

[2] Note that the shape of the histogram is sensitive to the choice of the width of the category bins.

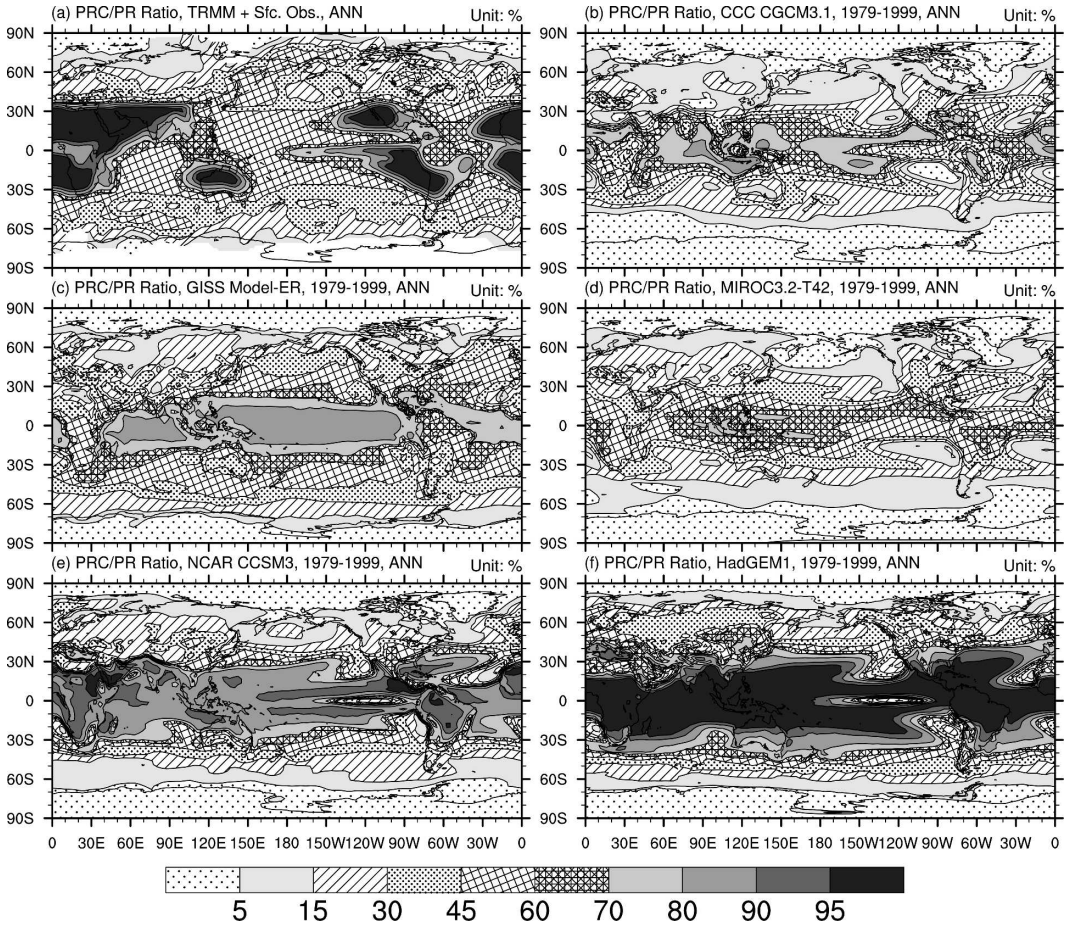

FIG. 11. Same as Fig. 10, except for convective to total precipitation ratio (%). Note the observed ratio outside 37°S–37°N is the showery to all-form (except drizzle) precipitation frequency ratio based on surface observations (from Dai 2001a).

days), compared with 75% in the TRMM data (Fig. 16). Excluding the very light precipitation ($\leq$1 mm day^{-1}), the models rain about 40%–55% of the days or 146–200 days yr^{-1}, whereas the TRMM data show a frequency of 29% or 106 days yr^{-1} (Fig. 16). Thus, the newest generation of CGCMs still rains too frequently, as in previous generations (e.g., Osborn and Hulme 1998; Dai and Trenberth 2004), mostly within the 1–10 mm day^{-1} categories, while heavy precipitation (>20 mm day^{-1}) occurs too rarely.

8. Precipitation diurnal cycle

Figure 17 shows the mean diurnal evolution of precipitation and its local time of the maximum of the diurnal harmonic, which is close to the time of the actual maximum (Dai et al. 1999; also see Fig. 17) of summer [June–August (JJA) + December–February (DJF) for the Tropics] precipitation from TRMM and surface observations and five models with 3-hourly data available. The TRMM-blended data have relatively short length of records and poor diurnal sampling by the TRMM instruments, while the surface observations of precipitation frequency were derived from 1975–97 records, although sampling over tropical and southern oceans were also sparse (Dai 2001a,b). Large differences exist between the two datasets, especially over the oceans where the TRMM data show a much weaker diurnal cycle with maxima around 0700–0800 local solar time (LST) compared with 0400–0600 LST in the surface observations (Fig. 17). The TRMM data lag the surface observations by a couple of hours over many land areas, and they are closer to the diurnal phase of surface-observed showery (i.e., convective) precipitation (Fig. 17). This is not unexpected, as the TRMM data used IR radiance measurements from geosynchronous satellites to derive the diurnal timing, and the IR radiance is a measure of high clouds generated from deep convection.

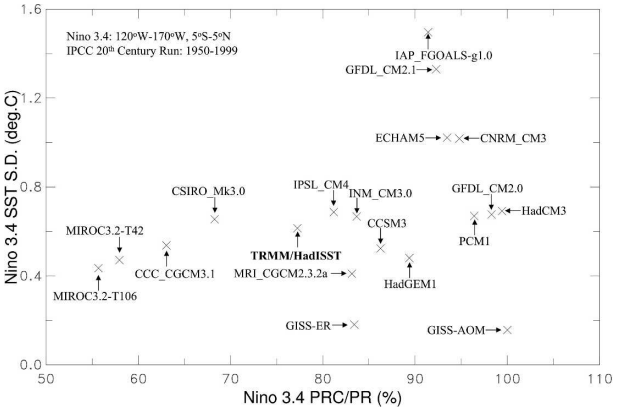

FIG. 12. Scatterplot of the (1950–99) standard deviation (°C) of the Niño-3.4 region (5°S–5°N, 120°–170°W) area-averaged annual SST vs the Niño-3.4 area-averaged values of annual convective-to-total precipitation ratio (%) from observations [1998–2003 TRMM precipitation and 1950–99 HadISST from Rayner et al. (2003)] and 18 coupled climate models. The correlation coefficient between the Nino-3.4 SST sd and PRC/PR ratio is 0.30 (p = 0.25) including all of the models, and 0.51 (p = 0.06) excluding the two GISS models and the IAP model.

Over land, the CCSM2 and MIROC3.2 show elevated precipitation from 1000 to 2000 LST without sharp peaks, while the GISS-ER, MRI-CGCM2.3.2a, and GFDL-CM2.0 have peak precipitation soon after noontime, in contrast to ~1600 LST in surface observations (Fig. 17). GISS-ER and, to a lesser extent, MRI-CGCM2.3.2a have too strong diurnal cycles over tropical land. Over the oceans, most models show weak diurnal cycles with peaks around 0200 LST (compared with 0400–0600 LST in surface observations) and amplitudes comparable to the TRMM data. The MIROC3.2 produces a relatively realistic diurnal phase compared with surface observations. These biases in precipitation diurnal variations suggest that warm-season convection still starts too early in all the new models, and is too frequent at reduced intensity in some models (e.g., CCSM2, MIROC3.2), as in previous CGCMs (Trenberth et al. 2003; Dai and Trenberth 2004).

9. Summary and concluding remarks

Monthly and 3-hourly precipitation data from the twentieth-century climate simulations in support of the IPCC Fourth Assessment by the newest generation of 18 coupled climate system models were analyzed and compared with observations, which include the global monthly precipitation from CMAP and GPCP v2, GPCP pentad precipitation, and 3-hourly data from TRMM and surface observations. The precipitation characteristics examined include mean spatial patterns; seasonal, year-to-year, and ENSO-related variability; convective versus stratiform precipitation ratio; daily precipitation frequency and intensity for different precipitation categories; and the diurnal cycle.

Most of the models reproduce the observed broad spatial pattern and annual cycle of precipitation. However, the newest models without flux corrections still show, to a varying degree, two zonal bands of maximum precipitation straddling the equator over the central and eastern Pacific, whereas in nature the rainfall double ITCZs occur only in boreal spring over the eastern Pacific. The two models (CGCM3.1 and MRI-CGCM2.3.2a) with flux corrections in the Tropics produce the most realistic rainfall patterns at low latitudes without the double ITCZs. Among the models without flux corrections, the MIROC3.2 and HadCM3 produce relatively realistic patterns of tropical precipitation.

The tropical rainfall biases are related to errors in simulated SST fields. The cold tongue in observed SST in the equatorial eastern Pacific extends too far to the central Pacific in most of the models without flux corrections. Associated with this extended SST cold tongue, an unrealistic narrow band of minimum precipitation exists over the equatorial central and eastern Pacific in all of these models, which contribute to the double-ITCZ pattern. The SST cold tongue fails to extend to the coast of South America in some models (e.g., FGOALS-g1.0 and HadCM3). Systematic SST biases also exist in many models (e.g., too warm in HadCM3, FGOALS-g1.0 and ECHAM5, but too cold in CNRM-CM3, MROC3.2, CSIRO-Mk3.0, and HadGEM1). Most models do not simulate well the distribution of mean total cloud amount, including marine stratus clouds, with the HadCM3 and HadGEM1 severely underestimating cloud cover over most of the globe. The SST and associated precipitation biases over the tropical Pacific likely result at least partly from errors in air–sea exchanges of energy and water (e.g., resulting from errors in cloud radiative feedbacks), while variations in the cumulus and large-scale precipitation parameterizations do not result in systematic differences in simulated precipitation.

The models generally reproduce the year-to-year variability of precipitation, with better sd distribution in models with more realistic mean precipitation patterns. The GFDL-CM2.0 and -CM2.1 both overestimate the sd in the equatorial central and western Pacific, while the GISS-AOM and GISS-ER models underestimate tropical precipitation variability. Many models, especially the GFDL-CM2.1, HadCM3, and ECHAM5, reproduce the horseshoe-shaped ENSO-related precipitation pattern originating from the Indonesia region

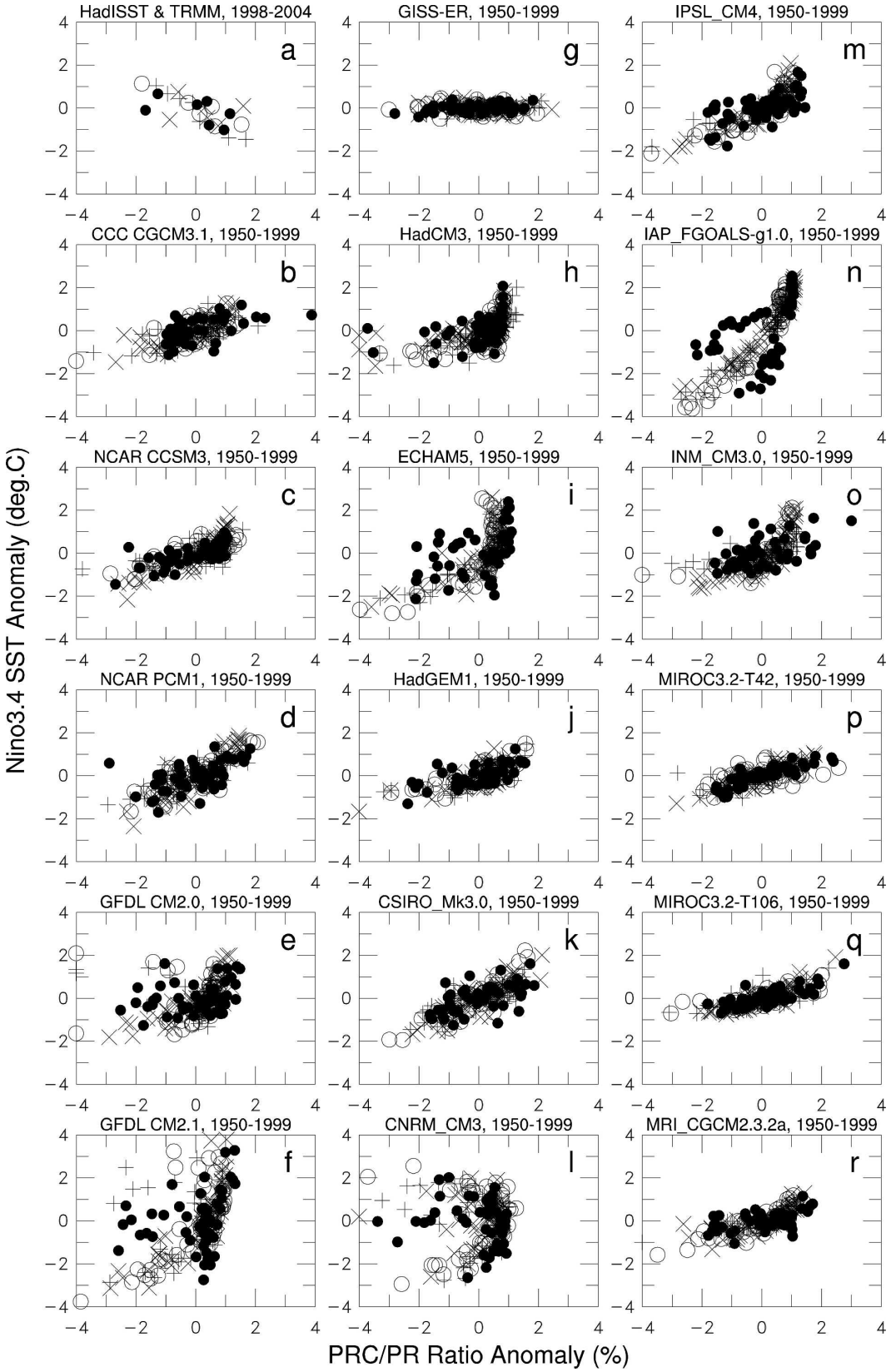

FIG. 13. Scatterplots of seasonal anomalies of the SST and PRC/PR (convective vs total precipitation) ratio averaged over the Niño-3.4 region (5°S–5°N, 120°–170°W) from (a) observations (HadISST and TRMM 3A25 precipitation (for 1998–2004) and (b)–(r) 17 models (for 1950–99). The different symbols represent different seasons.

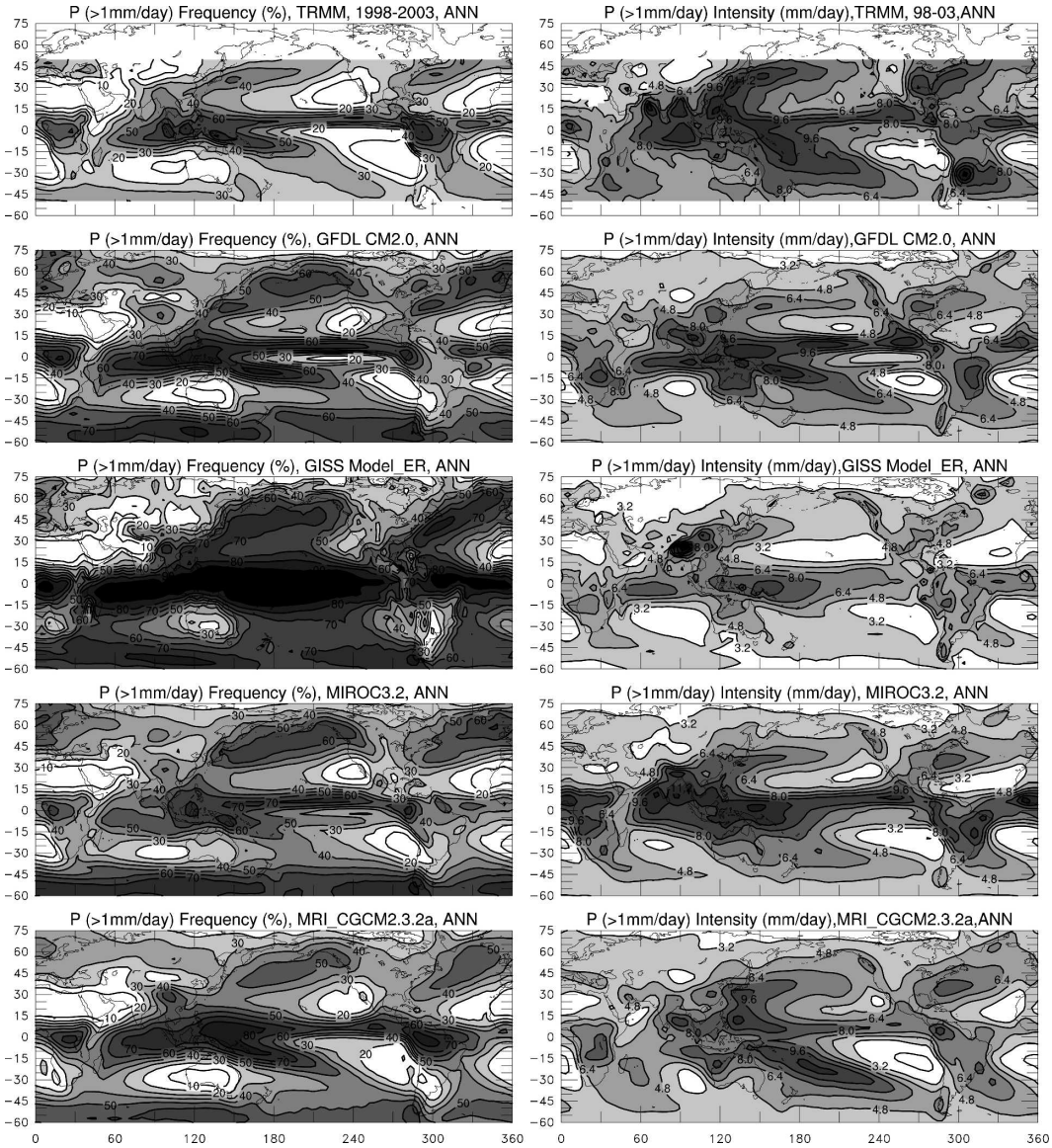

FIG. 14. (left) Annual-mean frequency (% of time) and (right) intensity (mm day^{-1}) of daily precipitation (>1 mm day^{-1}) events from TRMM satellite observations [(top) 3B42 dataset, 1998–2003 mean] and four coupled models (1991–2000 mean).

and extending northeast- and southeastward. The intraseasonal (20–80 day) variations account for the largest (20%–40%) percentage of the total variances of pentad precipitation, while the interannual variations contribute very little (<5%) except over the tropical Pacific where they are significant (10%–15%), resulting from ENSO. Seasonal (80–365 day) variations contribute 5%–20% to the total variance. The models reproduce these general partitioning, with substantial biases in South America and the tropical Pacific. The models reproduce the main features of the observed power spectra of pentad precipitation, although they fail to capture the large intraseasonal variations over the western Pacific.

Most models, especially the GFDL and Met Office models, GISS-AOM and PCM, produce too much convective (over 95% of total precipitation) and too little stratiform precipitation over most of the low latitudes, in contrast to the 45%–65% from convective precipitation in the TRMM satellite observations (excluding the subtropical dry regions), although the TRMM estimates contain uncertainties. The MIROC3.2, CGCM3.1, and GISS-ER produce relatively realistic stratiform precipitation fields. The biases in the convective versus strati-

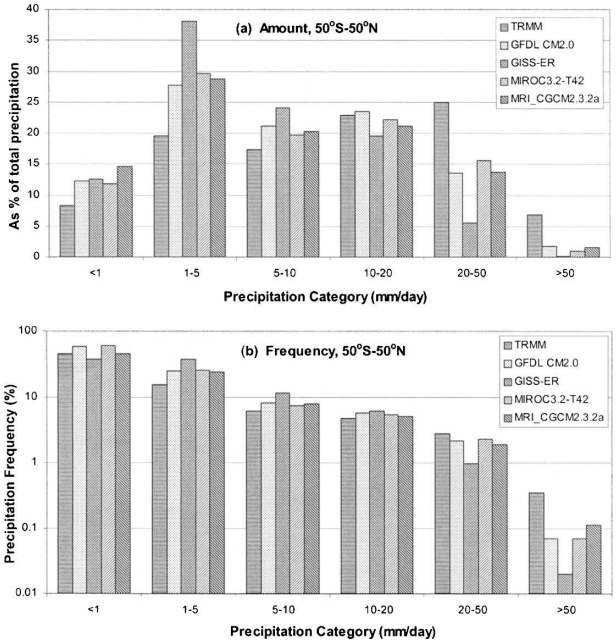

FIG. 15. (a) 50°S–50°N area-averaged percentage contribution to annual total precipitation amount by different precipitation categories from TRMM satellite observations (3B42 dataset, 1998–2003 mean) and four coupled models (1991–2002 mean). (b) 50°S–50°N area-averaged annual precipitation frequency (% of time, on a logarithmic scale) for different precipitation categories from TRMM and four models.

form precipitation ratio are linked to deficiencies in model-simulated ENSO amplitudes: the sd of ENSO SST indices increases with the tropical convective-to-total (PRC/PR) precipitation ratio among the models. This apparent intermodel relationship results from strong positive coupling between tropical convection and local SST in most models, in contrast to a negative correlation between Niño-3.4 SST and PRC/PR ratios suggested by the limited TRMM data.

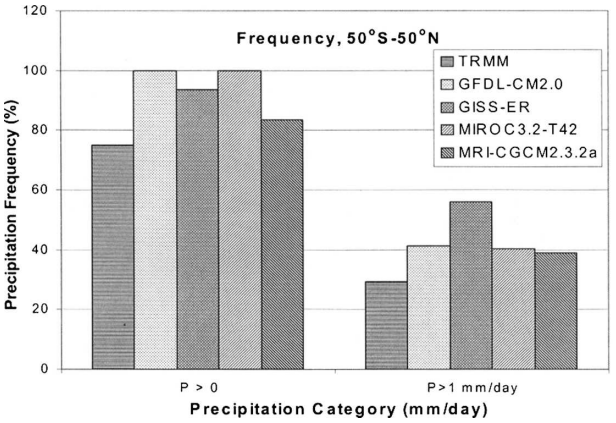

FIG. 16. Percentage of annual days within a year to have (left) nonzero and (right) >1 mm day^{-1} precipitation in the TRMM 3B42 dataset (1988–2003 mean) and four coupled models (1991–2002 mean).

The TRMM data show relatively uniform intensity (≈3–6 mm day^{-1}) of daily precipitation (>1 mm day^{-1}) over land, whereas daily precipitation frequency varies greatly from <5% in northern Africa and the Middle East to ~65% in the ITCZ and 70%–80% in northern South America and Indonesia. Daily precipitation over the storm tracks around the eastern coasts of Asia and North America has an intensity comparable to that in the ITCZ (10–12 mm day^{-1}), but with a lower frequency (~35%–50%). The GFDL-CM2.0, MIROC3.2, and MRI-CGCM2.3.2a reproduce the broad patterns of the daily precipitation frequency and intensity, while the GISS-ER severely overestimates the frequency and underestimates the intensity. The high-intensity bands around the storm tracks are too weak and their patterns are not well simulated by the models. The models reproduce the percentage contribution (to total precipitation) and frequency for moderate precipitation (10–20 mm day^{-1}), but underestimate the contribution and frequency for heavy (>20 mm day^{-1}) precipitation and overestimate them for light (<10 mm day^{-1}) precipitation. The newest generation of coupled models still rains too frequently, mostly within the 1–10 mm day^{-1} category, while heavy precipitation (>20 mm day^{-1}) occurs too rarely.

The diurnal phase in the TRMM-blended precipitation lags surface observations by 2–3 h, as the IR radiance used in the TRMM data measures high clouds generated from deep convection. Over land during summer, the GISS-ER, MRI-CGCM2.3.2a, and GFDL-CM2.0 show peak precipitation soon after noontime, in contrast to ~1600 LST in surface observations, whereas the CCSM2 and MIROC3.2 show elevated precipitation from 1000 to 2000 LST. Over oceans, most models show weak diurnal cycles with peaks around 0200 LST compared with 0400–0600 LST in surface observations. The MIROC3.2 produces relatively realistic diurnal phase compared with surface observations. The results suggest that warm-season convection still starts too early in the new models, and occurs too frequently at reduced intensity in some of the models (e.g., CCSM2, MIROC3.2).

We recognize that realistic simulations of global precipitation fields are a very challenging task, and that the latest generation of coupled climate system models has been improved considerably over their previous versions used just a few years ago in many aspects, such as avoiding climate drifts without surface flux corrections and increased resolution. However, regional and local impacts of future climate changes will most likely come

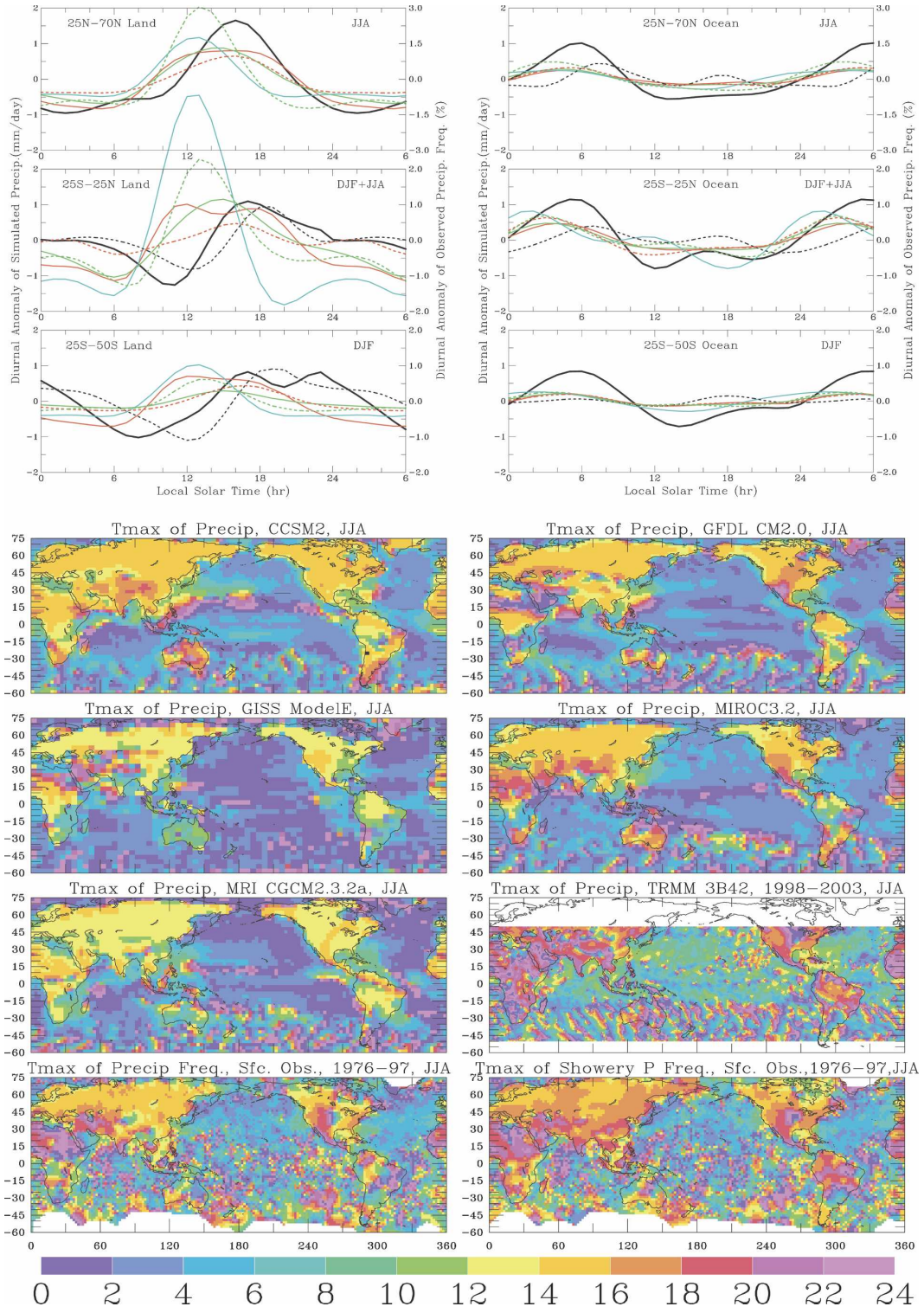

FIG. 17. (top) Mean diurnal cycle of precipitation from observations [black solid line: surface-observed precipitation frequency from Dai (2001b); black dashed line: TRMM 3B42 dataset, 1998–2003 mean] and five coupled models averaged at each local time over (left) land and (right) ocean within the indicated zones and seasons (JJA, DJF). Each colored curve is for one model: CCSM2 (red solid), GFDL-CM2.0 (green solid), GISS-ER (blue), MIROC3.2 (red dashed), and MRI-CGCM2.3.2a (green dashed). (bottom) Color maps of local solar time (h) of the maximum of the diurnal harmonic of JJA precipitation from five models and observations [TRMM and surface-observed nondrizzle and showery or convective precipitation frequencies from Dai (2001b), bottom panels].

from regional precipitation changes. Therefore, it is vital for these models to be able to realistically simulate the spatial pattern and other characteristics of precipitation, although offline (i.e., without two-way interactions) downscaling using regional climate models (e.g., Liang et al. 2006) may alleviate the impact of biases in regional precipitation from CGCMs on climate change assessments. The results of this study show that considerable improvements in this area are still desirable, for example, through improved representation of mountains and high terrain. Improvements in other model aspects, such as moist convection (e.g., Zhang and Wang 2006) and air–sea interactions (e.g., an improved diurnal cycle in surface oceans, see Danabasoglu et al. 2006), may reduce biases in tropical SST and precipitation fields. Our results show that many of the major precipitation biases seen in previous CGCMs, such as the double ITCZs associated with tropical SST biases, regional precipitation biases over complex terrain, and deficiencies in simulating intraseasonal and diurnal variations and the combination of frequency and intensity for light and heavy precipitation, still exist in current CGCMs. Further improvements in these areas will likely require higher model resolution (e.g., 30–60 km) and improved model physics (e.g., atmospheric convection, clouds, and air–sea interactions). The fact that all current CGCMs without flux corrections produce mean stable states with large systematic biases in tropical SST and rainfall fields suggests that it is a difficult task to realistically simulate tropical air–sea interactions. This is partly because small errors often lead to large biases through positive feedbacks. It might be desirable to ensure that coupled models contain certain negative feedbacks (as in nature) that would prevent small errors or anomalies from evolving into large systematic biases.

Acknowledgments. The author thanks two anonymous reviewers for constructive comments, and the modeling groups and the PCMDI for making the model data available. The IPCC Data Archive at Lawrence Livermore National Laboratory is supported by the U.S. Department of Energy (DOE) Office of Sciences. The TRMM data were acquired as part of the Tropical Rainfall Measuring Mission (TRMM), which was sponsored by the Japan National Space Development Agency (NASDA) and the U.S. National Aeronautics and Space Administration (NASA) Office of Earth Sciences. The author also thanks Jim Hansen of NASA GISS and Gabriel Lau of GFDL for their support in obtaining their model data. This study was supported by NSF SGER Grant ATM-0451587 and the NCAR Water Cycle Program.

REFERENCES

Adler, R. F., and Coauthors, 2003: The Version-2 Global Precipitation Climatology Project (GPCP) monthly precipitation analysis (1979–present). *J. Hydrometeor.,* **4,** 1147–1167.

Arakawa, A., and W. H. Schubert, 1974: Interaction of a cumulus cloud ensemble with the large-scale environment, Part I. *J. Atmos. Sci.,* **31,** 674–701.

Awaka, J., T. Iguchi, H. Kumagai, and K. Okamoto, 1997: Rain type classification algorithm for TRMM precipitation radar. *Proc. 1997 Int. Geoscience and Remote Sensing Symp.,* Singapore, IEEE, 1633–1635.

Betts, A. K., 1986: New convective adjustment scheme, Pt. 1, Observational and theoretical basis. *Quart. J. Roy. Meteor. Soc.,* **112,** 677–691.

——, and C. Jakob, 2002: Study of diurnal cycle of convective precipitation over Amazonia using a single column model. *J. Geophys. Res.,* **107,** 4732, doi:10.1029/2002JD002264.

Biggerstaff, M. I., and S. A. Listemaa, 2000: An improved scheme for convective/stratiform echo classification using radar reflectivity. *J. Appl. Meteor.,* **39,** 2129–2150.

Blackmon, M., and Coauthors, 2001: The Community Climate System Model. *Bull. Amer. Meteor. Soc.,* **82,** 2357–2376.

Bony, S., and K. A. Emmanuel, 2001: A parameterization of the cloudiness associated with cumulus convection: Evaluation using TOGA COARE data. *J. Atmos. Sci.,* **58,** 3158–3183.

Chen, M., R. E. Dickinson, X. Zeng, and A. N. Hahmann, 1996: Comparison of precipitation observed over the continental United States to that simulated by a climate model. *J. Climate,* **9,** 2223–2249.

——, P. Xie, J. E. Janowiak, and P. A. Arkin, 2002: Global land precipitation: A 50-yr monthly analysis based on gauge observations. *J. Hydrometeor.,* **3,** 249–266.

Collins, W. D., and Coauthors, 2006: The Community Climate System Model: CCSM3. *J. Climate,* **19,** 2122–2143.

Covey, C., K. M. Achutarao, U. Cubasch, P. Jones, S. J. Lambert, M. E. Mann, T. J. Phillips, and K. E. Taylor, 2003: An overview of results from the Coupled Model Intercomparison Project. *Global Planet. Change,* **37,** 103–133.

Dai, A., 2001a: Global precipitation and thunderstorm frequencies. Part I: Seasonal and interannual variations. *J. Climate,* **14,** 1092–1111.

——, 2001b: Global precipitation and thunderstorm frequencies. Part II: Diurnal variations. *J. Climate,* **14,** 1112–1128.

——, and T. M. L. Wigley, 2000: Global patterns of ENSO-induced precipitation. *Geophys. Res. Lett.,* **27,** 1283–1286.

——, and K. E. Trenberth, 2004: The diurnal cycle and its depiction in the community climate system model. *J. Climate,* **17,** 930–951.

——, I. Y. Fung, and A. D. Del Genio, 1997: Surface observed global land precipitation variations during 1900–88. *J. Climate,* **10,** 2943–2962.

——, F. Giorgi, and K. E. Trenberth, 1999: Observed and model simulated precipitation diurnal cycles over the contiguous United States. *J. Geophys. Res.,* **104,** 6377–6402.

——, T. M. L. Wigley, B. A. Boville, J. T. Kiehl, and L. E. Buja, 2001: Climates of the twentieth and twenty-first centuries simulated by the NCAR climate system model. *J. Climate,* **14,** 485–519.

Dai, F., R. Yu, X. Zhang, Y. Yu, and J. Li, 2005: Impacts of an improved low-level cloud scheme on the eastern Pacific ITCZ-cold tongue complex. *Adv. Atmos. Sci.,* **22,** 559–574.

Danabasoglu, G., W. G. Large, J. J. Tribbia, P. R. Gent, B. P.

Briegleb, and J. C. McWilliams, 2006: Diurnal coupling in the tropical oceans of CCSM3. *J. Climate,* **19,** 2347–2365.

Davey, M. K., and Coauthors, 2002: STOIC: A study of coupled model climatology and variability in tropical ocean regions. *Climate Dyn.,* **18,** 403–420.

Del Genio, A. D., and M.-S. Yao, 1993: Efficient cumulus parameterization for long-term climate studies: The GISS scheme. *The Representation of Cumulus Convection in Numerical Models,* K. Emanuel and D. Raymond, Eds., Amer. Meteor. Soc., 181–184.

——, ——, W. Kovari, and K. K. W. Lo, 1996: A prognostic cloud water parameterization for global climate models. *J. Climate,* **9,** 270–304.

Delworth, T. L., R. S. Stouffer, K. W. Dixon, M. J. Spelman, T. R. Knutson, A. J. Broccoli, P. J. Kushner, and R. T. Wetherald, 2002: Simulation of climate variability and change by the GFDL R30 coupled model. *Climate Dyn.,* **19,** 555–574.

——, and Coauthors, 2006: GFDL's CM2 global coupled climate models. Part 1: Formulation and simulation characteristics. *J. Climate,* **19,** 643–674.

Diansky, N. A., and E. M. Volodin, 2002: Simulation of present-day climate with a coupled atmosphere-ocean general circulation model (English translation). *Izv. Atmos. Ocean. Phys.,* **38,** 732–747.

Doherty, R., and M. Hulme, 2002: The relationship between the SOI and extended tropical precipitation in simulations of future climate change. *Geophys. Res. Lett.,* **29,** 1475, doi:10.1029/2001GL014601.

Emanuel, K. A., 1991: A scheme for representing cumulus convection in large-scale models. *J. Atmos. Sci.,* **48,** 2313–2335.

Emori, S., T. Nozawa, A. Numaguti, and I. Uno, 2001: Importance of cumulus parameterization for precipitation simulation over East Asia in June. *J. Meteor. Soc. Japan,* **79,** 939–947.

Flato, G. M., G. J. Boer, W. G. Lee, N. A. McFarlane, D. Ramsden, M. C. Reader, and A. J. Weaver, 2000: The Canadian Centre for Climate Modelling and Analysis Global Coupled Model and its climate. *Climate Dyn.,* **16,** 451–467.

Gates, W. L., and Coauthors, 1999: An overview of the results of the Atmospheric Model Intercomparison Project (AMIP I). *Bull. Amer. Meteor. Soc.,* **80,** 29–55.

Gordon, C., C. Cooper, C. A. Senior, H. T. Banks, J. M. Gregory, T. C. Johns, J. F. B. Mitchell, and R. A. Wood, 2000: The simulation of SST, sea ice extents and ocean heat transports in a version of the Hadley Centre coupled model without flux adjustments. *Climate Dyn.,* **16,** 147–168.

Gordon, H. B., and Coauthors, 2002: The CSIRO Mk3 Climate System Model. CSIRO Atmospheric Research Tech. Paper 60, 130 pp. [Available online at http://www.dar.csiro.au/publications/gordon_2002a.pdf.]

Grandpeix, J. Y., V. Phillips, and R. Tailleux, 2004: Improved mixing representation in Emanuel's convection scheme. *Quart. J. Roy. Meteor. Soc.,* **130,** 3207–3222.

Gregory, D., and P. R. Rowntree, 1990: A mass flux convection scheme with representation of cloud ensemble characteristics and stability dependent closure. *Mon. Wea. Rev.,* **118,** 1483–1506.

——, R. Kershaw, and P. M. Inness, 1997: Parameterization of momentum transport by convection II: Tests in single column and general circulation models. *Quart. J. Roy. Meteor. Soc.,* **123,** 1153–1183.

Gu, G. J., R. F. Adler, and A. H. Sobel, 2005: The eastern Pacific ITCZ during the boreal spring. *J. Atmos. Sci.,* **62,** 1157–1174.

Hasumi, H., and Coauthors, 2004: K-1 Coupled GCM (MIRCO) description. K-1 Model Developers Tech. Rep. 1, 34 pp. [Available online at http://www.ccsr.u-tokyo.ac.jp/kyosei/hasumi/MIROC/tech-repo.pdf.]

Houze, R. A. J., 1997: Stratiform precipitation in regions of convection: A meteorological paradox? *Bull. Amer. Meteor. Soc.,* **78,** 2179–2196.

Hulme, M., 1991: An intercomparison of model and observed global precipitation climatologies. *Geophys. Res. Lett.,* **18,** 1715–1718.

Jones, T., and Coauthors, 2005: HadGEM1—Model description and analysis of preliminary experiments for the IPCC Forth Assessment Report. Met Office Hadley Centre Tech. Note 55, 74 pp. [Available online at http://www.metoffice.com/research/hadleycentre/pubs/HCTN/HCTN_55.pdf.]

Kummerow, C., and Coauthors, 2000: The status of the Tropical Rainfall Measuring Mission (TRMM) after two years in orbit. *J. Appl. Meteor.,* **39,** 1965–1982.

Le Treut, H., and Z.-X. Li, 1991: Sensitivity of an atmospheric general circulation model to prescribed SST changes: Feedback effects associated with the simulation of cloud opitcal properties. *Climate Dyn.,* **5,** 175–187.

Li, J. L., X. H. Zhang, Y. Q. Yu, and F. S. Dai, 2004: Primary reasoning behind the double ITCZ phenomenon in a coupled ocean-atmosphere general circulation model. *Adv. Atmos. Sci.,* **21,** 857–867.

Liang, X.-Z., J. Pan, J. Zhu, K. E. Kunkel, J. X. L. Wang, and A. Dai, 2006: Regional climate model downscaling of the U.S. summer climate and future change. *J. Geophys. Res.,* **111,** D10108, doi:10.1029/2005JD006685.

Lietzke, C. E., C. Deser, and T. H. Vonder Haar, 2001: Evolutionary structure of the eastern Pacific double ITCZ based on satellite moisture profile retrievals. *J. Climate,* **14,** 743–751.

Lohmann, U., and E. Roeckner, 1996: Design and performance of a new cloud microphysics parameterization developed for the ECHAM4 general circulation model. *Climate Dyn.,* **12,** 557–572.

Marti, O., and Coauthors, 2005: The new IPSL climate system model: IPSL-CM4. Institut Pierre Simon Laplace Tech. Note 26, 84 pp. [Available online at http://dods.ipsl.jussieu.fr/omamce/IPSLCM4/DocIPSLCM4/FILES/DocIPSLCM4_color.pdf.]

Martin, G. M., and Coauthors, 2004: Evaluation of the atmospheric performance of HadGAM/GEM1. Met Office Hadley Centre Tech. Note 54, 64 pp. [Available online at http://www.metoffice.com/research/hadleycentre/pubs/HCTN/HCTN_54.pdf.]

McAvaney, B. J., and Coauthors, 2001: Model evaluation. *Climate Change 2001: The Scientific Basis,* J. T. Houghton et al., Eds., Cambridge University Press, 471–524.

Mechoso, C. R., and Coauthors, 1995: The seasonal cycle over the tropical Pacific in coupled ocean–atmosphere general circulation models. *Mon. Wea. Rev.,* **123,** 2825–2838.

Meehl, G. A., C. Covey, B. McAvaney, M. Latif, and R. J. Stouffer, 2005: Overview of the Coupled Model Intercomparison Project. *Bull. Amer. Meteor. Soc.,* **86,** 89–93.

Monahan, A. H., and A. Dai, 2004: The spatial and temporal structure of ENSO nonlinearity. *J. Climate,* **17,** 3026–3036.

Moorthi, S., and M. J. Suarez, 1992: Relaxed Arakawa-Schubert. A parameterization of moist convection for general circulation models. *Mon. Wea. Rev.,* **120,** 978–1002.

Nordeng, T. E., 1994: Extended versions of the convective param-

eterization scheme at ECMWF and their impact on the mean and transient activity of the model in the tropics. ECMWF Tech. Memo. 206, 41 pp.

Osborn, T. J., and M. Hulme, 1998: Evaluation of the European daily precipitation characteristics from the atmospheric model intercomparison project. *Int. J. Climatol.,* **18,** 505–522.

Pan, D. M., and D. A. Randall, 1998: A cumulus parametrization with a prognostic closure. *Quart. J. Roy. Meteor. Soc.,* **124,** 949–981.

Rasch, P. J., and Coauthors, 2006: A characterization of tropical transient activity in the CAM3 atmospheric hydrologic cycle. *J. Climate,* **19,** 2222–2242.

Rayner, N. A., D. E. Parker, E. B. Horton, C. K. Folland, L. V. Alexander, D. P. Rowell, E. C. Kent, and A. Kaplan, 2003: Global analyses of sea surface temperature, sea ice, and night marine air temperature since the late nineteenth century. *J. Geophys. Res.,* **108,** 4407, doi:10.1029/2002JD002670.

Ricard, J. L., and J. F. Royer, 1993: A statistical cloud scheme for use in an AGCM. *Ann. Geophys. Atmos. Hydrosph. Space Sci.,* **11,** 1095–1115.

Roeckner, E., and Coauthors, 2003: The atmospheric general circulation model ECHAM5. Part I: Model description. Max Planck Institute for Meteorology Rep. 349, 127 pp.

Rotstayn, L. D., 2000: On the "tuning" of autoconversion parameterizations in climate models. *J. Geophys. Res.,* **105,** 15 495–15 507.

Russell, G. L., J. R. Miller, and D. Rind, 1995: A coupled atmosphere-ocean model for transient climate change studies. *Atmos.-Ocean,* **33,** 683–730.

Schmidt, G. A., and Coauthors, 2006: Present day atmospheric simulations using GISS ModelE: Comparison to in situ, satellite and reanalysis data. *J. Climate,* **19,** 153–192.

Schumacher, C., and R. A. Houze Jr., 2003: Stratiform rain in the Tropics as seen by the TRMM precipitation radar. *J. Climate,* **16,** 1739–1756.

——, ——, and I. Kraucunas, 2004: The tropical dynamical response to latent heating estimates derived from the TRMM precipitation radar. *J. Atmos. Sci.,* **61,** 1341–1358.

Smith, R. N. B., 1990: A scheme for predicting layer clouds and their water content in a general circulation model. *Quart. J. Roy. Meteor. Soc.,* **116,** 435–460.

Srinivasan, G., M. Hulme, and C. G. Jones, 1995: An evaluation of the spatial and interannual variability of tropical precipitation as simulated by GCMs. *Geophys. Res. Lett.,* **12,** 2139–2142.

Sun, D. Z., J. Fasullo, T. Zhang, and A. Roubicek, 2003: On the radiative and dynamical feedbacks over the equatorial Pacific cold tongue. *J. Climate,* **16,** 2425–2432.

Sun, Y., S. Solomon, A. Dai, and R. Portmann, 2005: How often does it rain? *J. Climate,* **19,** 916–934.

Tiedtke, M., 1989: A comprehensive mass flux scheme for cumulus parameterization in large-scale models. *Mon. Wea. Rev.,* **117,** 1779–1800.

——, 1993: Representation of clouds in large-scale models. *Mon. Wea. Rev.,* **121,** 3040–3061.

Trenberth, K. E., A. Dai, R. M. Rasmussen, and D. B. Parsons, 2003: The changing character of precipitation. *Bull. Amer. Meteor. Soc.,* **84,** 1205–1217.

Washington, W. M., and Coauthors, 2000: Parallel climate model (PCM) control and transient simulations. *Climate Dyn.,* **16,** 755–774.

Wilson, D. R., and S. P. Ballard, 1999: A microphysically based precipitation scheme for the UK Meteorological Office Unified Model. *Quart. J. Roy. Meteor. Soc.,* **125,** 1607–1636.

Xie, P., and P. A. Arkin, 1997: Global precipitation: A 17-year monthly analysis based on gauge observations, satellite estimates, and numerical model outputs. *Bull. Amer. Meteor. Soc.,* **78,** 2539–2558.

Xie, S. C., and Coauthors, 2002: Intercomparison and evaluation of cumulus parametrizations under summertime midlatitude continental conditions. *Quart. J. Roy. Meteor. Soc.,* **128,** 1095–1135.

——, M. H. Zhang, J. S. Boyle, R. T. Cederwall, G. L. Potter, and W. Y. Lin, 2004: Impact of a revised convective triggering mechanism on Community Atmosphere Model, Version 2, simulations: Results from short-range weather forecasts. *J. Geophys. Res.,* **109,** D14102, doi:10.1029/2004JD004692.

Yanai, M., J.-H. Chu, T. E. Starx, and T. Nitta, 1976: Response of deep and shallow tropical maritime cumuli to large-scale processes. *J. Atmos. Sci.,* **33,** 976–991.

Yu, Y., X. Zhang, and Y. Guo, 2004: Global coupled ocean-atmosphere general circulation models in LASG/IAP. *Adv. Atmos. Sci.,* **21,** 444–455.

Yukimoto, S., and Coauthors, 2006: Present-day climate and climate sensitivity in the Meteorological Research Institute Coupled GCM, Version 2.3 (MRI-CGCM2.3). *J. Meteor. Soc. Japan,* **84,** 333–363.

Zhang, C. D., 2001: Double ITCZs. *J. Geophys. Res.,* **106,** 11 785–11 792.

Zhang, G. J., 2003: Roles of tropospheric and boundary layer forcing in the diurnal cycle of convection in the U.S. Southern Great Plains. *Geophys. Res. Lett.,* **30,** 2281, doi:1029/2003GL018554.

——, and N. A. McFarlane, 1995: Sensitivity of climate simulations to the parameterization of cumulus convection in the Canadian Climate Centre general circulation model. *Atmos.-Ocean,* **33,** 407–446.

—— and H. Wang, 2006: Toward mitigating the double ITCZ problem in NCAR CCSM3. *Geophys. Res. Lett.,* **33,** L06709, doi:10.1029/2005GL025229.

Zhang, M., W. Lin, C. B. Bretherton, J. J. Hack, and P. J. Rasch, 2003: A modified formulation of fractional stratiform condensation rate in the NCAR Community Atmosphere Model (CAM2). *J. Geophys. Res.,* **108,** 4035, doi:10.1029/2002JD002523.